

Original paper

Compositional variations in tourmalines from peraluminous rocks of the Dipilto Granitic Batholith, Eastern Chortis Terrane, Nicaragua: tracers of magmatic to hydrothermal evolution

David BURIÁNEK^{1*}, Vladimír ŽÁČEK²¹ Czech Geological Survey, Leitnerova 22, 658 59 Brno, Czech Republic; david.burianek@geology.cz² Czech Geological Survey, Klárov 3, 118 21 Prague 1, Czech Republic

*Corresponding author



The granitoids of the Dipilto Batholith in northern Nicaragua range in composition from amphibole–biotite tonalite to cordierite–biotite and biotite granite. The petrographic and geochemical features indicate hybrid origin for the metaluminous granodiorite and tonalite (El Paraiso Suite). Dominant peraluminous granites (leucogranite dykes, Yumpali and La Piedra suites) represent a typical product of fractional crystallization of crust-derived melts.

Tourmaline occurs as rare mineral in peraluminous granites of the Yumpali Suite (randomly distributed grains and quartz–tourmaline nodules), but is common in the younger leucogranite, pegmatite dykes and hydrothermal veins. Chemical variations (mainly X_{Fe} and F) in tourmaline as well as in biotite are consistent with magmatic differentiation processes in granites and pegmatites. The presence of quartz–tourmaline hydrothermal veins indicates involvement of B-rich post-magmatic hydrothermal fluids at the final stage of the Dipilto Batholith evolution. Tourmaline chemistry evolved from Mg-rich schorl in peraluminous granites, to F-rich schorl–foitite in the hydrothermal veins. This evolutionary trend is typical of F-poor granite–pegmatite systems.

Keywords: tourmaline, pegmatite, granite, geochemistry, Dipilto Batholith, Nicaragua

Received: 12 March 2014; **accepted:** 3 February 2015; **handling editor:** Milan Novák

The online version of this article (doi: 10.3190/jgeosci.189) contains supplementary electronic material.

1. Introduction

Tourmaline is a common accessory-to-minor mineral in peraluminous granitoids, pegmatites and associated hydrothermal veins. Its chemical composition depends on the origin and evolution of the parental magma or fluid phases (Henry and Guidotti 1985). Tourmaline may have crystallized during the early magmatic evolution of granitic rocks (London et al. 1996), through early subsolidus to hydrothermal conditions (e.g., Pichavant and Manning 1984; Sinclair and Richardson 1992; London and Manning 1995; London et al. 1996; Williamson et al. 2000; Dini et al. 2007). Chemical zonation in tourmaline crystals of magmatic and hydrothermal origins is different (e.g., London 1999). A number of studies have shown that there exists link between textural position and chemical composition of tourmalines in the granitic bodies (e.g., Sinclair and Richardson 1992; Broska et al. 1998; Kubiš and Broska 2005; Buriánek and Novák 2007). Changes in tourmaline chemical composition primarily depend on many factors such as degree of fractionation of granitic melts, temperature and B content in the melt or fluids (London et al. 1996; London 1999). Therefore, tourmaline can potentially be used in interpretation of the evolution of boron-rich magmatic

systems (London et al. 1996; Wolf and London 1997; Kubiš and Broska 2005).

In our contribution, we characterize a wide range of textural types of tourmalines related to Cretaceous peraluminous granites in the Dipilto Batholith, Nicaragua. These rocks are suitable for studying the behaviour of boron at various stages of granitic systems development: from magmatic crystallization to the subsolidus conditions.

The Dipilto Batholith has been previously interpreted as petrographically relatively homogeneous granite intrusion (Hradecký et al. 2005, and the references therein). However, we describe several types of granitoids with distinct evolution in this paper. According to field observations, coupled with petrography and geochemistry, the Dipilto Batholith can be described as a composite intrusion of hybrid origin. The chemical and mineralogical characteristics indicate that metasediments represented a major source for the tourmaline granite. However, interaction with hybrid and/or basic magma strongly affected distribution and textural diversity of tourmaline in the granitic melt (e.g., Balen and Broska 2011). Therefore behaviour of the boron-rich melt is difficult to interpret without understanding evolution of all igneous suites in the Dipilto Batholith.

2. Geological setting

The Dipilto Batholith is situated at the Honduras–Nicaragua state border (Fig. 1a). This area pertains to the eastern part of the Chortis Block (Eastern Chortis Terrane), which consists of slightly metamorphosed carbonate and siliciclastic sediments intruded by Cretaceous plutonic rocks (Ritchie and Finch 1985; Rogers 2003; Buriánek and Dolníček 2011). The Eastern Chortis Terrane belongs to the rifted continental margin of the North American Plate developed during the Jurassic separation of the North and South American plates (e.g., Dengo 1969; Rogers 2003; Rogers et al. 2007).

The NE–SW trending Dipilto Batholith (Fig. 1b) represents one of the largest plutonic bodies in the Eastern Chortis Terrane. The main part of this batholith is situated between the towns of Ocotal and Jalapa in northern Nicaragua. The modal composition of plutonic rocks ranges from diorites, granodiorites to granites with subor-

inated gabbros. The dominant rock types are porphyritic biotite granites to granodiorites (Yumpali Suite) locally with cordierite and/or tourmaline (Fig. 2a–b); however, in NE part of batholith, biotite and amphibole–biotite granodiorites to tonalites (El Paraiso Suite) predominate. Boundaries between El Paraiso and Yumpali suites are transitional and interfingered. Medium-grained biotite to muscovite granites (La Piedra Suite) form small bodies inside the porphyritic biotite granites to granodiorites. Numerous tourmaline-bearing leucogranite, aplite and pegmatite dykes and small stocks occur in the Dipilto Batholith and within its metamorphic aureole. Radiometric dating indicates a Cretaceous intrusion age of the Dipilto Batholith (Zoppis-Bracci and Del Giudice 1961; Donnelly et al. 1990; Hodgson 2000). The Rb–Sr whole-rock age 140 ± 15 Ma (Donnelly et al. 1990) represents the best estimate of the emplacement age and K–Ar ages (110 ± 1.2 Ma on biotite and 115 ± 1.5 Ma on hornblende; Hodgson 2000) are interpreted as cooling ages.

This intrusive body is surrounded by a contact aureole several km wide. The country rock represents a metasedimentary sequence, interpreted as a metamorphosed lithological equivalent of the Jurassic Agua Fria Fm. (Viland et al. 1996) or a part of the Nueva Segovia Paleozoic metasedimentary sequences (Palacagüina Fm.; Zoppis-Bracci 1957; Figge 1966; Hradecký et al. 2005).

The main host rocks are graphitic metapelites with layers of metapsammites. In addition, intercalations of metavolcanites, metaconglomerates, quartzites and calc-silicate rocks occur locally. Relics of sedimentary textures, such as lamination, bedding and/or positive gradation in metapsammitic layers in the western part of the studied area are often preserved. The contact-metamorphic assemblage is relatively simple: cordierite + biotite + graphite \pm muscovite \pm K-feldspar \pm andalusite \pm chlorite (Buriánek

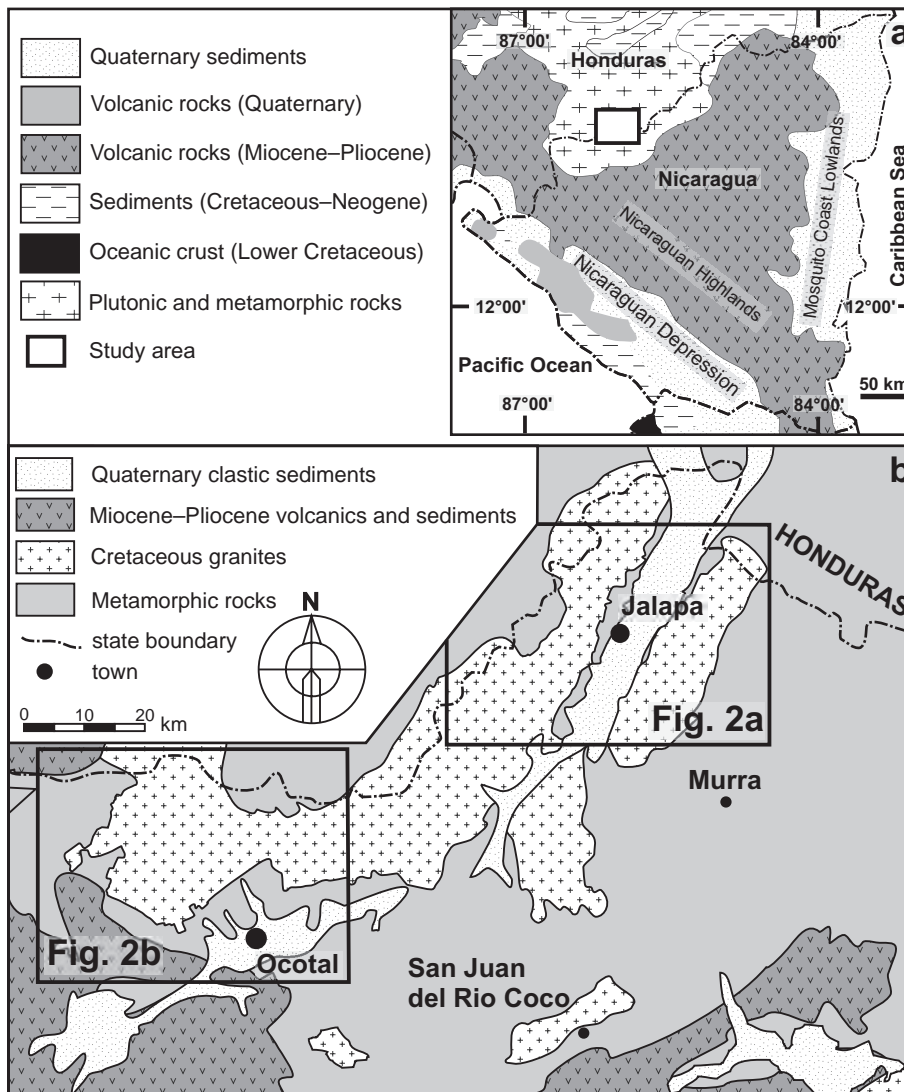


Fig. 1 Simplified geological maps of Nicaragua (a) and of the Dipilto Batholith (b). After Rogers (2003), Žáček and Hradecký (2005), Rogers et al. (2007), Buriánek et al. (2010), modified.

and Dolníček 2011). Three main stages of ductile deformation were distinguished in the contact aureole of the Dipilto Batholith (Buriánek and Dolníček 2011). The first deformation phase D_1 was related to low-grade regional metamorphism and was followed by D_2 accompanied by emplacement of the Dipilto Batholith at depths of c. 6 km. Deformation event D_3 formed subsolidus foliation in granitoids oriented ~ NNW–SSE with steep dip to the E–NE.

3. Analytical techniques

3.1. Electron microprobe

Electron-microprobe analyses (EMPA) were performed by R. Čopjaková with the Cameca SX-100 instrument at the Joint Laboratory of Electron Microscopy and Microanalysis of Masaryk University and the Czech Geological Survey (Brno, Czech Republic). The measurements were carried out using a wave-dispersion mode under the following conditions: accelerating voltage of 15 kV, beam current of 10 nA for tourmaline, feldspar and mica, and 20 nA for garnet; beam diameter of 5 μm for tourmaline, feldspar and mica, and <1 μm for garnet. Natural and synthetic standards were used (Si, Al – sanidine, Mg – olivine, Fe – almandine, Ca – andradite, Mn – rhodonite, Ti – Ti-hornblende, Cr – chromite, Na – albite, K – orthoclase, P – apatite, F – topaz, Cl, V – vanadinite, Zn – gahnite, Cu – metallic Cu, Y – YAG). The raw concentration data were corrected using the method of Pouchou and Pichoir (1985).

The empirical formulae of cordierite, feldspars and micas were recalculated to 18, 8 and 22 oxygen atoms, respectively,

assuming that all Fe is present as Fe^{2+} . The empirical formulae of tourmalines were calculated on the basis of 15 Y + Z + T cations; the O^{2-} content in the W-site was obtained from the charge-balanced formula ($\text{OH} = 4 - \text{F} - \text{W}\text{O}$ apfu, B = 3 apfu). The garnet formulae were obtained on the basis of 12 oxygen atoms; the ferric iron contents were estimated based on charge balance and stoichiometry (Droop 1987). The amphibole formulae were calculated on the basis of 23 oxygen atoms (Leake et al. 1997). The $\text{Fe}^{2+}/\text{Fe}^{3+}$ ratios were estimated assum-

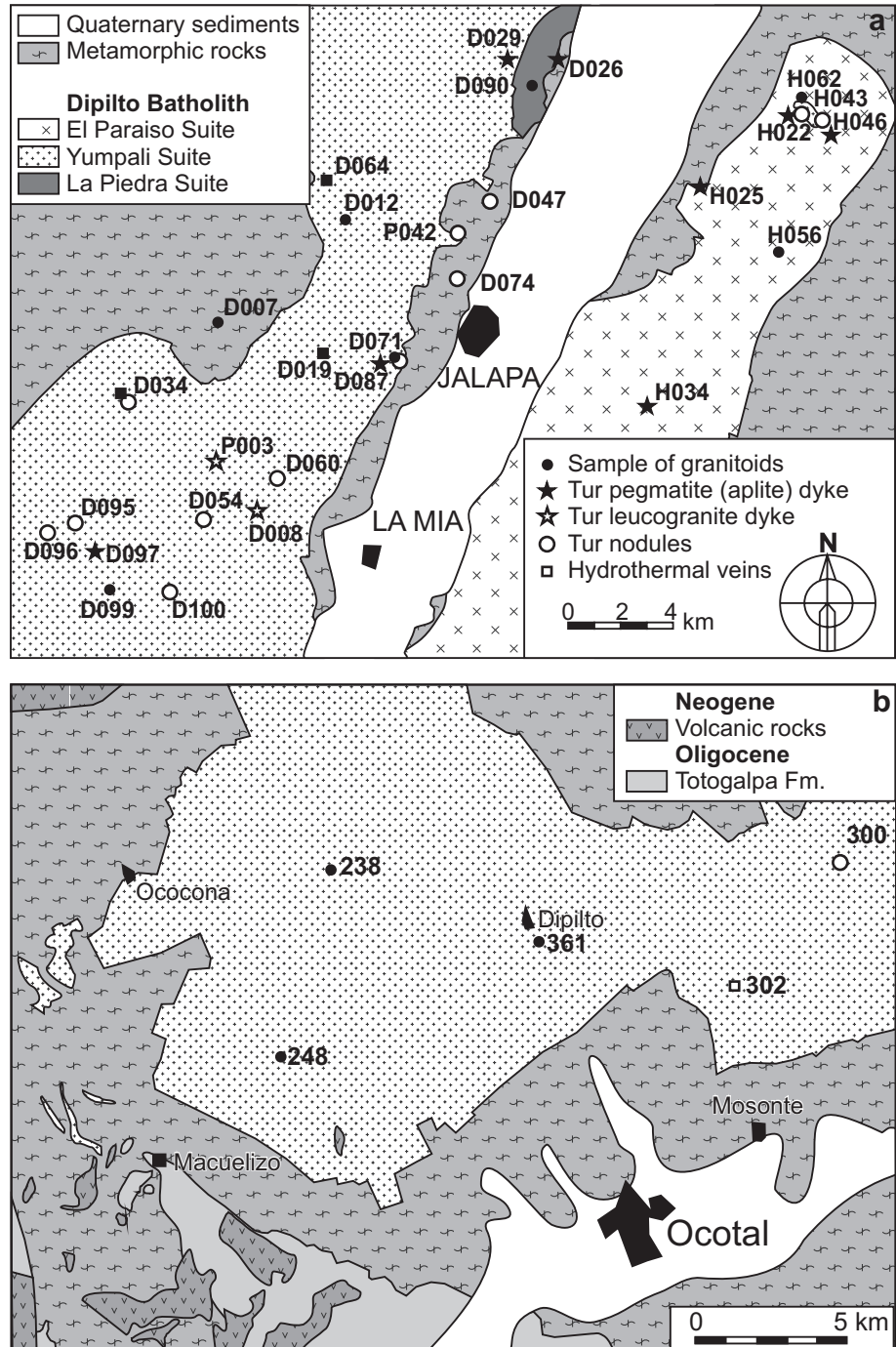


Fig. 2 Simplified geological map of the northeastern (a) and southwestern (b) parts of the Dipilto Batholith with sample locations (Tab. 1).

ing the cation sum = 13 atoms without Ca, Na and K (13 eCNK). The abbreviations of the mineral names used in the text are taken from Kretz (1983) and Whitney and Evans (2010).

3.2. Whole-rock geochemistry

Twenty-two samples (3–4 kg) represent all the main petrogenetic types rocks of the Dipilto Batholith including 10 samples of tourmaline-bearing rocks (Tab. 1). Most whole-rock chemical analyses were carried out at Acme Analytical Laboratories, Vancouver, Canada. Major-element oxides were determined by the ICP-OES method. Loss on ignition (LOI) was calculated from the weight difference after heating to 1000 °C. The rare earth and other trace elements were analysed by INAA and ICP-MS following LiBO₂ fusion. The whole-rock chemical analyses 238, 248, 300, 361 were performed in the laboratories of the Czech Geological Survey in Prague (Dempírová 2010; Dempírová et al. 2010). Because of differences in the analytical methods (Nb, Y, Zr and U were analysed by X-ray fluorescence; Sr, Ba, Cs, Rb, Zn, V and Ni by atomic absorption spectrometry and Co, Cr, Cu, Ga, Mo, Pb, Zn by optical emission spectrometry) only major oxides and some trace elements were used in this work.

Geochemical data were recalculated and plotted using the *GCDkit* software package (Janoušek et al. 2006). The

fractional crystallization in rocks of Dipilto Batholith was interpreted using a FC–AFC–FCA and mixing modeller (Ersoy and Helvacı 2010). Fractional crystallization trends were interpreted using crystal/melt partition coefficients for K-feldspar, plagioclase and biotite recommended for granite by Ersoy and Helvacı (2010).

4. Petrography of plutonic rocks of the Dipilto Batholith

The Dipilto Batholith is a body about 130 km long and 40 km wide that crops out over several thousands of km², consisting of four main igneous suites (Žáček and Hradecký 2005; Buriánek et al. 2010; Fig. 2a–b; Tab. 2): (1) biotite and amphibole–biotite granodiorites to tonalites, which locally contain abundant mafic enclaves or bodies, (2) porphyritic biotite granites to granodiorites locally with cordierite and/or tourmaline, (3) medium-grained biotite to muscovite granites, (4) leucocratic dykes and stocks (leucogranites to pegmatites).

4.1. Biotite and amphibole–biotite granodiorite to tonalite (El Paraiso Suite)

The El Paraiso Suite is exposed in NE–SW elongated body east of Jalapa and La Mia (Fig. 2a). Dominant bio-

Tab. 1 Location of the studied samples

Sample	Longitude (°E)	Latitude (°N)	Locality	Rock	Suite
D008*	–86.1908	13.8624	Lugar Aguas Calientes	Bt granite (Tur nod.)	Yumpali
D012*	–86.1656	13.9500	El Escambray	Bt granite	Yumpali
D034	–86.2391	13.8981	Casa Quemada	Tur–Qtz vein	Yumpali
D041	–86.1483	13.9074	Loma El Trompo	Tur pegmatite	Leucogranite
D064*	–86.1716	13.9637	Cerro Jesús	Bt granite	Yumpali
D071*	–86.1577	13.9094	Yumpali	Crd–Bt granite	Yumpali
D071C*	–86.1577	13.9094	Yumpali	leucogranite (Tur)	Leucogranite
D090	–86.1031	13.9919	Cerro La Piedra	Bt granite	Yumpali
D095	–86.2547	13.8572	La Ceiba	Crd–Bt granite (Tur nod.)	Yumpali
D099*	–86.2430	13.8364	Lugar Plan El Hornito	Bt granite	Yumpali
D107*	–86.2076	13.9189	Río Arriba	Bt granite	Yumpali
H022*	–86.0147	13.9860	Poza Redonda	Amp–Bt gabbro	El Paraiso
H045*	–86.0008	13.9683	Cerro los Esclavos	Bt granite (Tur nod.)	La Piedra
H046*	–86.0035	13.9737	Cerro Los Esclavos	Tur granite	Leucogranite
H056*	–86.0118	13.9384	Río Macaralí	Amp–Bt granodiorite	El Paraiso
H064	–86.0319	13.9328	Río Macaralí	Ms–Bt granite	La Piedra
H034	–86.0100	13.8942	Cerro Casa Fuego	Bt granite (Tur nod.)	Yumpali
238**	–86.5776	13.7364	Rodeo Grande	Amp–Bt tonalite	El Paraiso
248**	–86.5830	13.6848	Macuelizo	Bt tonalite	El Paraiso
300**	–86.4141	13.7361	Mosonte	Bt granite (Tur nod.)	Yumpali
302	–86.4460	13.6893	Mosonte	Tur veinlet in granite	Yumpali
361**	–86.5052	13.7130	Dipilto	Bt granite	Yumpali

Whole-rock chemical analyses performed in:

* Acme Analytical Laboratories, Vancouver, Canada

** laboratories of the Czech Geological Survey in Prague

nod. = nodules, Tur = tourmaline, Bt = Biotite, Amp = amphibole, Crd = cordierite

Tab. 2 Main features of the individual granitoid suites making up the Dipilto Batholith

Group	basic rocks	H _m and H _{ss} -type granitoids	H _s and S-type granitoids	S-type granitoids
Suite	El Paraiso	El Paraiso	Yumpali, La Piedra	leucogranite dykes
Rock types	Amp and Amp-Bt gabbro to diorite	Amp-Bt tonalite to Bt granodiorite	Bt to Crd-Bt granite to granodiorite	Tur to Ms-Bt aplite, pegmatite and granite
Texture	medium-grained hypidiomorphic	medium-grained hypidiomorphic	medium to coarse-grained sometimes porphyritic metasedimentary	fine to coarse-grained, variable textures
Enclaves	–	igneous (diorite to gabbro)	(restite and hornfelses)	–
Occurrence	enclaves (up to several m)	mainly eastern part of the batholith	western part of the batholith	dykes up to 1 m thick
Rock-forming minerals	Amp + Pl ± Bt	Bt + Pl + Qtz + Kfs ± Amp	Bt + Pl + Qtz + Kfs ± Cdr	Bt + Pl + Qtz + Kfs ± Tur ± Ms
Accessory minerals	Ap, Mnz, Ilm, Mag	Ap, Mnz, Zrn, Ilm, Ttn	Tur, Grt, Ap, Mnz, Zrn, Ilm	Ap, Mnz, Zrn, Grt
Secondary minerals	Ep, Chl, Cal, Scp, sericite	Chl, Cal, Prh, Hem, zeolite	Prh, Chl, sericite	Chl, sericite
ZST (W-H 1983)	–	743–777 °C	746–843 °C	653–739 °C
Major elements (wt. %)				
SiO ₂	49–60	63–69	69–75	73
CaO	6.6–12.5	3.3–4.1	1.0–2.3	0.6–0.2
K ₂ O	0.8–1.5	2.8–3.3	3.7–6.1	5.2–5.7
FeO/MgO	0.7–1.6	1.9–2.7	3.1–6.9	4.6–7.7
A/CNK	0.68–0.77	0.94–0.97	0.95–1.30	1.30–1.43
Trace elements (ppm)				
Rb	32–62	83–107	161–263	197–242
Ba	155–231	90–555	546–1988	96–675
Sr	214–498	227–433	49–156	20–85
Th	2.3–2.6	9.4	11.6–18.8	7.7–4.3
Zr/Hf	33–35	32	32–36	20–31
Nb	2–10	7–11	8–17	3–12
La	7–11	13–24	24–40	5–18

granitoid classification after Castro et al. (1991)

ZST (W-H 1983) = zircon saturation thermometry (Watson and Harrison 1983)

tite and amphibole-biotite granodiorites to tonalites are grey, medium-grained (Fig. 3a), occasionally porphyritic rocks. Volumetrically subordinated gabbros or diorites form stocks, up to 80 m in diameter, but mostly occur as elongated enclaves up to 30 cm long enclosed by granodiorites and tonalites of the El Paraiso Suite.

Tonalites to granodiorites consist of subhedral to euhedral plagioclase (35–49 vol. %), anhedral quartz (25–31 vol. %), perthitic K-feldspar (1–8 vol. %), biotite (8–14 vol. %) and amphibole (0–8 vol. %). K-feldspar (Or_{92–96}Ab_{4–8}) is relatively homogenous whereas plagioclase frequently displays an oscillatory-zoned pattern (sometimes with resorption zones) and occasionally preserves boxy-cellular cores (An_{27–54}). Homogeneous biotite (X_{Fe} = 0.53–0.54, ^{IV}Al = 2.41–2.45 apfu; Fig. 4a) and slightly heterogeneous magnesiohornblende (Mg/(Mg + Fe) = 0.55–0.61, Si = 7.13–7.41 apfu) are present. Accessory zircon, monazite and apatite mostly occur as small inclusions in biotite. The secondary minerals include clinozoisite, prehnite and muscovite partially replacing plagioclase cores.

Mostly subangular mafic enclaves (Fig. 3a) are randomly distributed in host rocks. They are medium- to fine-grained and occasionally porphyritic with mi-

crogranular structure. Their groundmass consists of plagioclase, biotite and amphibole with plagioclase megacrysts.

Medium- to coarse-grained amphibole and amphibole-biotite gabbro usually form small bodies, up to 50 m in diameter, composed of dominant magnesiohornblende (55–73 vol. %) and plagioclase (23–45 vol. %) with more or less continuously normally zoned cores (often surrounded by a resorption zone) and oscillatory-zoned rim (An_{32–45}). Subhedral to anhedral magnesiohornblende grains (Mg/(Mg + Fe) = 0.59–0.63, Si = 7.16–7.25 apfu) are locally replaced by actinolite. Subordinated, (0–4 vol. %), partially chloritized biotite (annite with X_{Fe} = 0.53–0.54, ^{IV}Al = 2.41–2.48 apfu; Fig. 4a) often contains small inclusions of amphibole. Epidote, clinozoisite and prehnite are secondary minerals.

4.2. Porphyritic biotite granites to granodiorites locally with cordierite and/or tourmaline (Yumpali Suite)

The pinkish-grey porphyritic granites to granodiorites of the Yumpali Suite (Fig. 3b) dominate western part of the Dipilto Batholith (Fig. 2a–b). They consist mainly

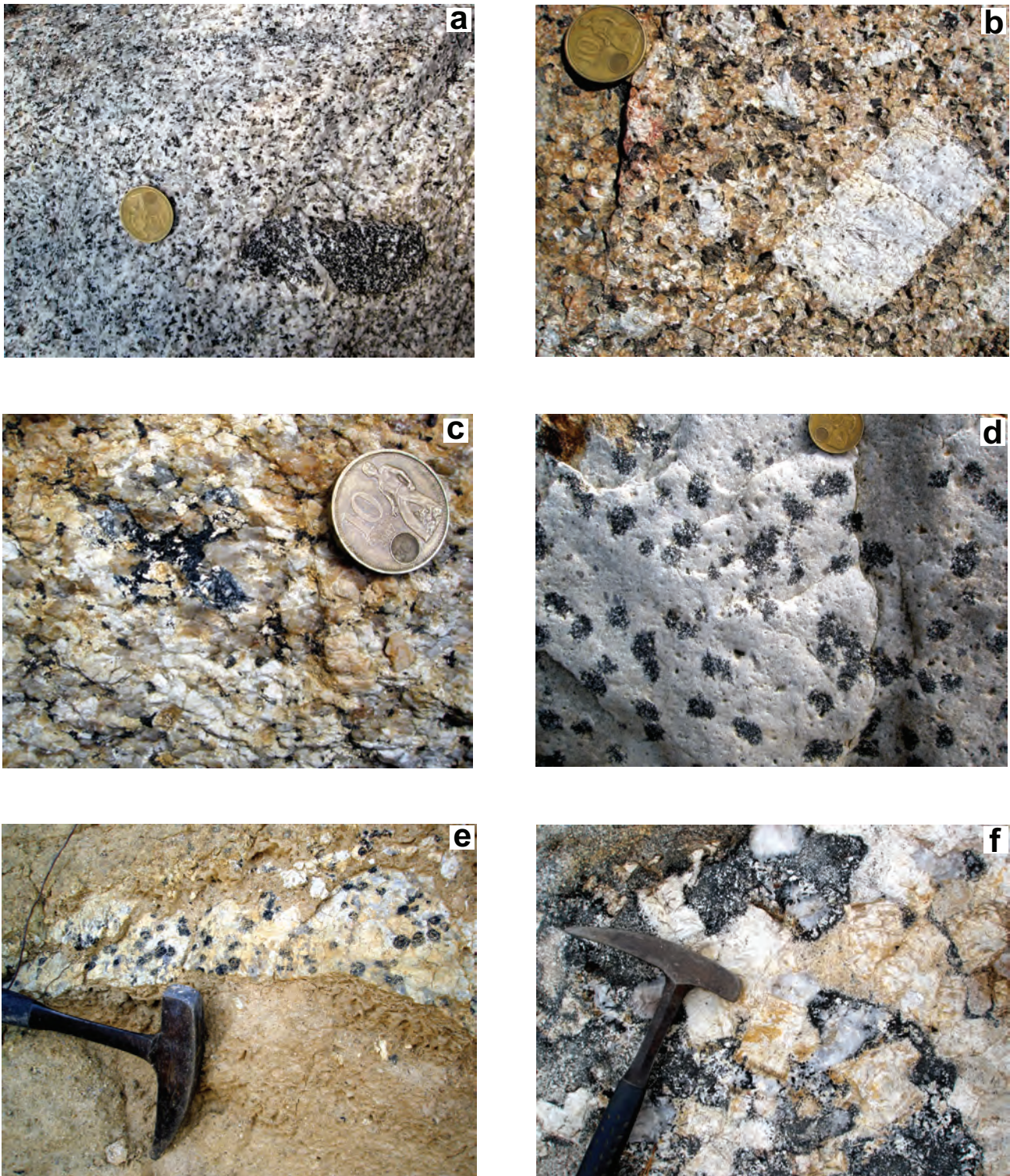


Fig. 3 Field characteristics of the Dipilto Batholith. **a** – Mafic microgranular enclave in the tonalite, H056 (El Paraiso Suite); **b** – K-feldspar phenocryst in biotite granite with cordierite, D071 (Yumpali Suite); **c** – Incipient tourmaline nodule in the biotite granite with cordierite (tourmaline partially replaced by feldspar and thus the leucocratic halo is indistinct), D034 (Yumpali Suite); **d** – Leucogranite with small tourmaline nodules; **e** – Pegmatitic dyke with tourmaline in strongly weathered granite, D092; **f** – Quartz and tourmaline in the central parts of pegmatitic miaroles, H022.

of groundmass anhedral quartz (30–35 vol. %), fine- to medium-grained K-feldspar ($Or_{92-90}Ab_{9-10}$; 27–36 vol. %), subhedral to euhedral plagioclase (oscillatory-zoned and

sometimes resorbed plagioclase; An_{12-39} ; 24–29 vol. %), biotite (annite; $X_{Fe} = 0.59-0.61$, $^{IV}Al = 2.62-2.70$ apfu; Tab. 3) and occasional cordierite ($X_{Fe} = 0.46-0.52$). In ad-

Tab. 3 Representative electron-microprobe analyses of biotite (wt. % and apfu on the basis of 22 oxygens + 2 OH groups)

	D071/60	H056B2	H056B1	D090/39	D107B/54	D071B1	D071B2	D071B3
SiO ₂	34.49	35.85	35.78	34.89	36.02	34.93	34.62	34.65
TiO ₂	4.14	3.65	3.77	2.33	3.38	4.64	3.49	2.48
Al ₂ O ₃	18.83	14.05	14.03	18.74	17.86	17.63	18.78	19.01
FeO	21.91	20.93	20.88	21.29	19.57	20.81	19.77	19.15
MnO	0.37	0.28	0.28	0.23	0.28	0.21	0.39	0.39
MgO	6.01	10.17	10.15	8.20	8.62	7.56	8.36	9.42
CaO	0.01	0.14	0.10	0.00	0.00	0.07	0.01	0.00
Na ₂ O	0.13	0.07	0.11	0.07	0.13	0.21	0.12	0.08
K ₂ O	9.31	9.01	9.05	9.67	9.21	9.11	9.64	9.39
H ₂ O*	3.78	3.83	3.82	3.79	3.68	3.75	3.80	3.76
F	0.18	0.00	0.00	0.21	0.46	0.27	0.20	0.27
Cl	0.08	0.05	0.09	0.04	0.14	0.07	0.08	0.06
O=F,Cl	0.09	0.01	0.02	0.10	0.22	0.13	0.10	0.13
Total	99.15	98.01	98.04	99.37	99.14	99.12	99.15	98.53
Si	5.328	5.590	5.580	5.364	5.485	5.369	5.309	5.321
Ti	0.481	0.428	0.442	0.270	0.387	0.536	0.402	0.286
^{IV} Al	2.672	2.410	2.420	2.636	2.515	2.631	2.691	2.679
^{VI} Al	0.756	0.173	0.159	0.761	0.692	0.562	0.704	0.764
Fe	2.831	2.729	2.723	2.738	2.493	2.675	2.536	2.460
Mn	0.048	0.036	0.037	0.029	0.037	0.028	0.050	0.051
Mg	1.383	2.365	2.360	1.880	1.956	1.731	1.911	2.156
Ca	0.002	0.024	0.017	0.000	0.000	0.011	0.002	0.000
Na	0.039	0.020	0.034	0.022	0.039	0.062	0.034	0.024
K	1.835	1.792	1.800	1.897	1.789	1.786	1.885	1.840
S Cat	15.376	15.567	15.572	15.597	15.394	15.392	15.525	15.581
OH*	3.892	3.986	3.975	3.889	3.743	3.850	3.885	3.855
F	0.088	0.000	0.000	0.100	0.220	0.133	0.095	0.129
Cl	0.020	0.014	0.025	0.011	0.036	0.017	0.020	0.017

dition, 10–50 mm long euhedral K-feldspar phenocrysts are also present. Muscovite is rare and usually occurs as a secondary mineral in feldspars.

Tourmaline (Tab. 4) forms small subhedral randomly distributed grains or small nodules (Fig. 3c) with leucocratic halos up to several cm in diameter. Tourmaline nodules (up to 25 cm across) are mostly concentrated in 5–20 m thick zones located mainly at the batholith margins. The nodules are composed of two distinct zones: the central zone (a) and a leucocratic halo (b). The centre (a) consists of tourmaline (40–76 vol. %) and quartz (21–35 vol. %), with variable amounts of plagioclase (2–19 vol. %), K-feldspar (1–18 vol. %), and fluorapatite. The leucocratic biotite-free halo (b) surrounds the majority of the nodules. Accessory phases of tourmaline nodules include zircon, apatite, monazite, xenotime and ilmenite.

Metamorphic xenoliths, which are occasionally present in the Yumpali Suite, vary widely in size (< 1 to 40 cm) and shape (rounded to angular and irregular). They are mostly represented by cordierite hornfels and cordierite-rich restites. Xenoliths of calc-silicate rocks, amphibolites and biotite–plagioclase mafic microgranular enclaves are scarce. More than 90 % of all the observed enclaves in the Yumpali Suite are hornfels xenoliths. They exhibit characteristic fine- to medium-

grained equigranular mosaic textures. Biotite (annite; $X_{\text{Fe}} = 0.53–0.57$, ${}^{\text{IV}}\text{Al} = 2.68–2.69$ apfu; Fig. 4a), cordierite and normally zoned plagioclase ($\text{An}_{36–49}$) are the main constituents. Quartz and needles of sillimanite are scarce. Cordierite-bearing restitic enclaves are granoblastic to lepidoblastic and medium- to coarse-grained. The mineral assemblages are dominated by biotite (annite; $X_{\text{Fe}} = 0.52–0.55$, ${}^{\text{IV}}\text{Al} = 2.69$ apfu; 30–70 vol. %) and cordierite ($X_{\text{Fe}} = 0.56–0.57$, 15–60 vol. %) with subordinated plagioclase, quartz, sillimanite, hercynite and rare almandine-rich garnet ($\text{Alm}_{69}\text{Prp}_{22}\text{Sps}_5\text{Adr}_4$) frequently replaced by biotite.

4.3. Medium-grained biotite to muscovite granites (La Piedra Suite)

The granites of the La Piedra Suite contain mainly plagioclase (28–39 vol. %), quartz (30–35 vol. %), K-feldspar (15–30 vol %) and biotite (2–8 vol %). Euhedral to subhedral plagioclase phenocrysts have homogeneous or rare boxy-cellular cores ($\text{An}_{28–34}$) and albite-rich rims (< An_{12}). Subhedral K-feldspar ($\text{Or}_{92–90}\text{Ab}_{8–10}$) and biotite (annite; $X_{\text{Fe}} = 0.59–0.61$, ${}^{\text{IV}}\text{Al} = 2.62–2.68$ apfu; see Fig. 4a) are chemically relatively homogeneous. Garnet and/or muscovite are accessory minerals.

Tab. 4 Representative electron-microprobe analyses of tourmaline (wt. % and apfu on the basis of 15 Y + Z + T cations)

Sample	type I			type II			type III			type IV			type V									
	D095/53	300/1	H046/39	H046/40	H046/41	D071/70	D071/71	D071/72	D071/73	D071/75	D041/36	D041/37	D041/38	D041/39	D034/22	D034/24	D034/25	D034/29	D034/31	D107/17	D107/18	
SiO ₂	34.53	35.79	35.23	35.48	35.66	34.96	34.39	35.16	35.65	35.95	35.22	34.96	35.48	36.04	34.84	34.96	34.50	34.86	34.76	37.30	36.76	
TiO ₂	1.25	1.32	0.29	0.32	0.57	1.14	1.22	1.02	1.34	0.81	0.43	0.53	0.24	0.19	0.65	0.64	0.86	0.78	0.98	0.53	0.81	
Al ₂ O ₃	31.10	31.91	34.54	34.76	34.15	33.80	33.80	33.54	33.77	34.31	35.39	34.61	35.79	35.41	33.14	32.35	31.87	32.94	31.66	34.54	34.32	
V ₂ O ₅	–	–	–	–	0.04	0.06	0.04	0.04	0.04	–	–	–	–	–	–	–	0.03	–	–	–	0.08	0.13
FeO	14.64	12.58	12.64	12.28	10.93	11.22	11.93	10.94	10.31	8.58	13.87	14.00	13.03	13.35	15.55	15.01	15.01	14.40	14.42	7.44	7.29	
MgO	2.60	2.65	1.62	1.62	2.82	2.96	2.61	3.41	3.10	4.27	2.20	0.76	0.81	0.68	0.56	1.10	1.56	1.22	2.23	4.89	5.15	
CaO	0.73	0.63	0.12	0.11	0.21	0.49	0.59	0.59	0.31	0.26	0.04	0.19	0.13	0.08	0.29	0.31	0.41	0.42	0.44	0.29	0.42	
MnO	0.08	0.12	0.22	0.19	0.10	0.10	0.12	0.10	0.09	0.08	0.27	0.10	0.11	0.10	0.13	0.10	0.14	0.08	0.10	0.01	0.03	
ZnO	0.08	–	–	0.10	–	0.12	0.12	–	0.13	–	0.17	0.17	0.11	–	0.10	–	0.14	–	0.17	0.11	–	
Na ₂ O	2.14	2.20	1.67	1.63	1.84	1.80	1.71	1.76	1.64	1.68	1.43	1.62	1.41	1.38	1.91	2.12	2.30	1.99	2.31	1.47	1.58	
K ₂ O	0.06	0.09	0.04	0.03	0.04	0.04	0.06	0.06	–	0.03	0.04	–	–	–	0.04	0.05	0.04	0.06	0.07	0.03	0.02	
F	0.38	–	0.25	0.26	0.27	0.17	0.25	0.30	0.00	0.00	0.22	0.09	0.07	0.00	0.68	0.65	0.78	0.66	0.76	0.00	0.00	
H ₂ O*	3.13	2.92	3.15	3.11	3.04	3.13	3.13	3.09	3.13	3.23	3.12	3.21	3.21	3.19	2.90	2.82	2.84	2.79	2.90	3.23	3.20	
B ₂ O ₃ *	10.24	10.31	10.35	10.38	10.40	10.39	10.34	10.41	10.42	10.50	10.37	10.34	10.44	10.45	10.24	10.18	10.18	10.22	10.24	10.67	10.63	
O=F	0.16	0.00	0.10	0.11	0.11	0.07	0.10	0.13	0.00	0.00	0.09	0.04	0.03	0.00	0.29	0.27	0.33	0.28	0.32	0.00	0.00	
Total	100.79	100.54	100.01	100.15	99.93	100.29	100.20	100.28	99.93	99.71	100.67	100.54	100.81	100.87	100.74	100.02	100.32	100.14	100.72	100.58	100.33	
Site T+Z+Y																						
Si ⁴⁺	5.861	6.034	5.917	5.939	5.958	5.849	5.781	5.872	5.948	5.951	5.904	5.880	5.906	5.996	5.911	5.970	5.893	5.928	5.898	6.075	6.013	
TAl ³⁺	0.139	0.000	0.083	0.061	0.042	0.151	0.219	0.128	0.052	0.049	0.096	0.120	0.094	0.004	0.089	0.030	0.107	0.072	0.102	0.000	0.000	
ZAl ³⁺	6.000	6.000	6.000	6.000	6.000	6.000	6.000	6.000	6.000	6.000	6.000	6.000	6.000	6.000	6.000	6.000	6.000	6.000	6.000	6.000	6.000	
YAl ³⁺	0.082	0.340	0.753	0.796	0.682	0.513	0.478	0.475	0.588	0.645	0.894	0.740	0.927	0.937	0.538	0.479	0.308	0.531	0.230	0.632	0.615	
Ti ⁴⁺	0.159	0.168	0.036	0.040	0.071	0.143	0.154	0.128	0.168	0.101	0.054	0.067	0.030	0.024	0.083	0.083	0.111	0.099	0.124	0.065	0.099	
V ³⁺	0.000	0.000	0.000	0.000	0.005	0.008	0.006	0.005	0.005	0.000	0.000	0.000	0.000	0.000	0.000	0.000	0.004	0.000	0.000	0.011	0.017	
Fe ²⁺	2.078	1.773	1.774	1.719	1.527	1.570	1.677	1.528	1.439	1.188	1.944	1.969	1.814	1.857	2.206	2.144	2.144	2.049	2.046	1.014	0.996	
Mg ²⁺	0.659	0.667	0.404	0.405	0.701	0.737	0.653	0.850	0.771	1.054	0.049	0.190	0.200	0.168	0.142	0.279	0.396	0.310	0.564	1.188	1.256	
Mn ²⁺	0.012	0.017	0.032	0.027	0.014	0.014	0.017	0.014	0.013	0.012	0.038	0.014	0.016	0.013	0.019	0.015	0.020	0.011	0.015	0.002	0.004	
Zn ²⁺	0.010	0.000	0.000	0.012	0.000	0.014	0.015	0.000	0.017	0.000	0.021	0.021	0.014	0.000	0.012	0.000	0.017	0.000	0.021	0.013	0.000	
Site X																						
Ca ²⁺	0.132	0.115	0.022	0.020	0.038	0.087	0.107	0.105	0.055	0.046	0.008	0.035	0.024	0.015	0.052	0.056	0.075	0.077	0.081	0.050	0.073	
Na ⁺	0.706	0.721	0.543	0.527	0.597	0.583	0.556	0.571	0.532	0.540	0.465	0.528	0.455	0.445	0.628	0.702	0.763	0.657	0.758	0.463	0.502	
K ⁺	0.012	0.019	0.009	0.007	0.007	0.008	0.012	0.012	0.000	0.007	0.007	0.000	0.000	0.000	0.008	0.011	0.009	0.013	0.015	0.005	0.005	
vac.	0.150	0.146	0.427	0.446	0.358	0.321	0.325	0.312	0.413	0.408	0.520	0.437	0.521	0.540	0.312	0.231	0.153	0.253	0.146	0.481	0.420	
Site W+V																						
OH	3.550	3.287	3.531	3.473	3.392	3.489	3.513	3.440	3.482	3.564	3.489	3.603	3.568	3.545	3.282	3.209	3.232	3.161	3.282	3.507	3.492	
F ⁻	0.206	0.000	0.132	0.137	0.141	0.089	0.132	0.158	0.000	0.000	0.118	0.047	0.038	0.000	0.364	0.351	0.419	0.357	0.408	0.000	0.000	
O ²⁻	0.244	0.713	0.338	0.391	0.467	0.422	0.355	0.402	0.518	0.436	0.394	0.350	0.394	0.455	0.354	0.440	0.349	0.482	0.311	0.493	0.508	
B ³⁺	3.000	3.000	3.000	3.000	3.000	3.000	3.000	3.000	3.000	3.000	3.000	3.000	3.000	3.000	3.000	3.000	3.000	3.000	3.000	3.000	3.000	

type I = tourmaline nodules in granites of the Yumpali Suite, type II = tourmaline in the leucogranite dykes, type III = tourmaline of pegmatite dykes, type IV = tourmaline of quartz veins, type V = tourmaline in the contact metamorphic aureole

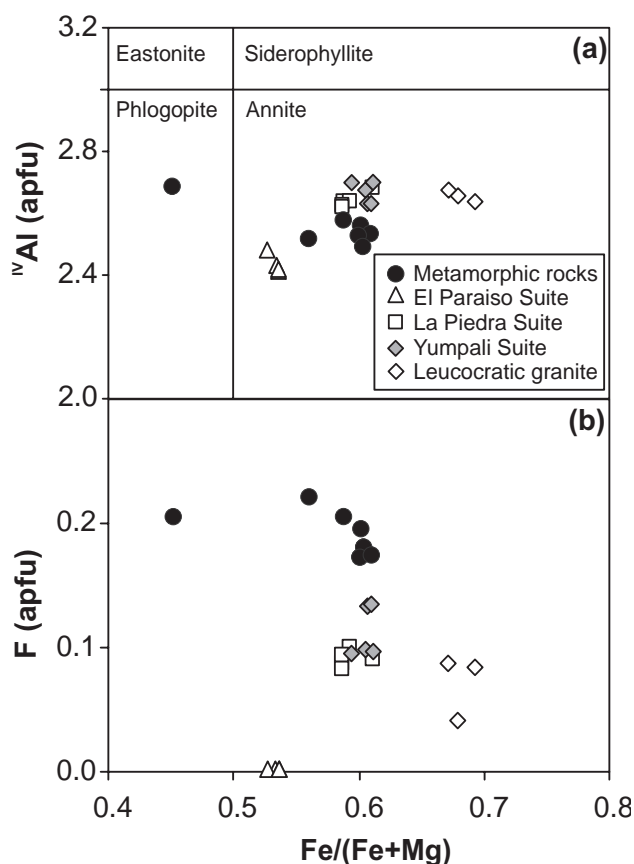


Fig. 4 Chemical composition of biotite in **a** – $\text{Fe}/(\text{Fe} + \text{Mg})$ vs. ^{14}Al and **b** – $\text{Fe}/(\text{Fe} + \text{Mg})$ vs. F plots.

Up to several cm long biotite- and cordierite–biotite restitic enclaves are locally abundant. They are composed of over 40 vol. % biotite (annite; $X_{\text{Fe}} = 0.55\text{--}0.59$, $^{14}\text{Al} = 2.59\text{--}2.64$ apfu), plagioclase (up to 30 vol. %) with patchy zoning ($\text{An}_{22\text{--}46}$) and various amounts of cordierite, hercynite and almandine-rich garnet ($\text{Alm}_{68\text{--}69}$ $\text{Prp}_{22\text{--}23}$ $\text{Sps}_{4\text{--}5}$ $\text{Adr}_{5\text{--}4}$ $\text{Grs}_{0\text{--}1}$).

4.4. Leucogranites, aplites and pegmatites

Tourmaline to muscovite–biotite leucogranites, aplites and pegmatites form several cm to m thick dykes or small stocks up to 600 m in diameter intruded into all remaining igneous suites and metasediments in the roof pedants of the Dipilto Batholith (Fig. 3d). Leucogranites are rich in subhedral quartz (30–38 vol. %) and perthitic K-feldspar ($\text{Or}_{89\text{--}91}$ $\text{Ab}_{9\text{--}11}$; 25–40 vol. %). Weakly normally zoned plagioclase ($\text{An}_{4\text{--}11}$; 20–25 vol. %) is partly altered to secondary muscovite. Biotite (up to 12 vol. %; $X_{\text{Fe}} = 0.67\text{--}0.69$, $^{14}\text{Al} = 2.64\text{--}2.67$ apfu; Fig. 4a) is frequently altered to chlorite. Muscovite ($X_{\text{Fe}} = 0.66\text{--}0.96$, $\text{Si} = 6.07\text{--}6.20$ apfu) is rare. Anhedral tourmaline is concentrated in nodules, up to 4 cm in diameter (Fig. 3d), or forms small subhedral grains disseminated in the rock occasionally associated with euhedral almandine–spessartine ($\text{Alm}_{47\text{--}67}$ $\text{Sps}_{30\text{--}52}$ $\text{Prp}_{1\text{--}2}$ $\text{Adr}_{0\text{--}1}$ $\text{Grs}_{0\text{--}1}$; grains up to 5 mm).

Medium- to coarse-grained pegmatites form dykes, up to 1 m wide, consisting of K-feldspar, albite, quartz and tourmaline (Fig. 3e–f), the latter forming euhedral columnar crystals (Fig. 3e). Occasionally is present magmatic layering with K-feldspar crystals oriented perpendicular to the individual layers. Fine-grained aplites consist of K-feldspar, albite, quartz and biotite or tourmaline. The tourmaline usually occurs in nodules or nests, up to 3 cm in diameter.

5. Geochemistry of granitoids

Based on the R_1 vs. R_2 classification diagram (De la Roche et al. 1980), studied rocks correspond to tonalite to granodiorite (El Paraiso Suite), granodiorite to granite (Yumpali Suite) and granite (La Piedra Suite) (Fig. 5a, Tab. 5). All the granitoids are calc-alkaline (Irvine and

Tab. 5 Major-element analyses of representative rocks from the Dipilto Batholith (in wt. %)

Suite	Yumpali			La Piedra		Leucogranite		El Paraiso	
Sample	D008	D012	D071	H045	D064	D071/C	H046	H022	H056/A
SiO_2	71.75	70.81	69.10	73.37	67.03	73.34	73.24	49.30	71.47
TiO_2	0.35	0.52	0.71	0.24	0.54	0.18	0.03	0.51	0.45
Al_2O_3	14.52	14.16	14.34	13.78	14.66	14.95	15.21	17.76	14.13
Fe_2O_3	2.17	3.24	4.21	2.10	4.34	1.52	1.28	6.91	2.94
MnO	0.04	0.06	0.06	0.05	0.09	0.04	0.08	0.13	0.07
Cr_2O_3	<0.002	0.003	0.006	<0.002	0.008	<0.002	<0.003	0.019	0.004
MgO	0.49	0.79	1.21	0.41	2.11	0.30	0.15	8.30	0.73
CaO	1.35	2.27	2.03	1.39	4.11	0.62	0.23	12.54	1.70
Na_2O	2.78	3.12	2.31	2.97	2.80	2.67	3.09	1.47	3.04
K_2O	5.06	3.96	4.40	4.72	2.84	5.18	5.72	0.78	4.36
P_2O_5	0.10	0.15	0.23	0.10	0.13	0.15	0.06	0.09	0.13
LOI	1.2	0.7	1.1	0.7	1.1	0.9	0.9	1.9	0.8
Sum	99.81	99.78	99.71	99.83	99.80	99.85	99.99	99.70	99.79

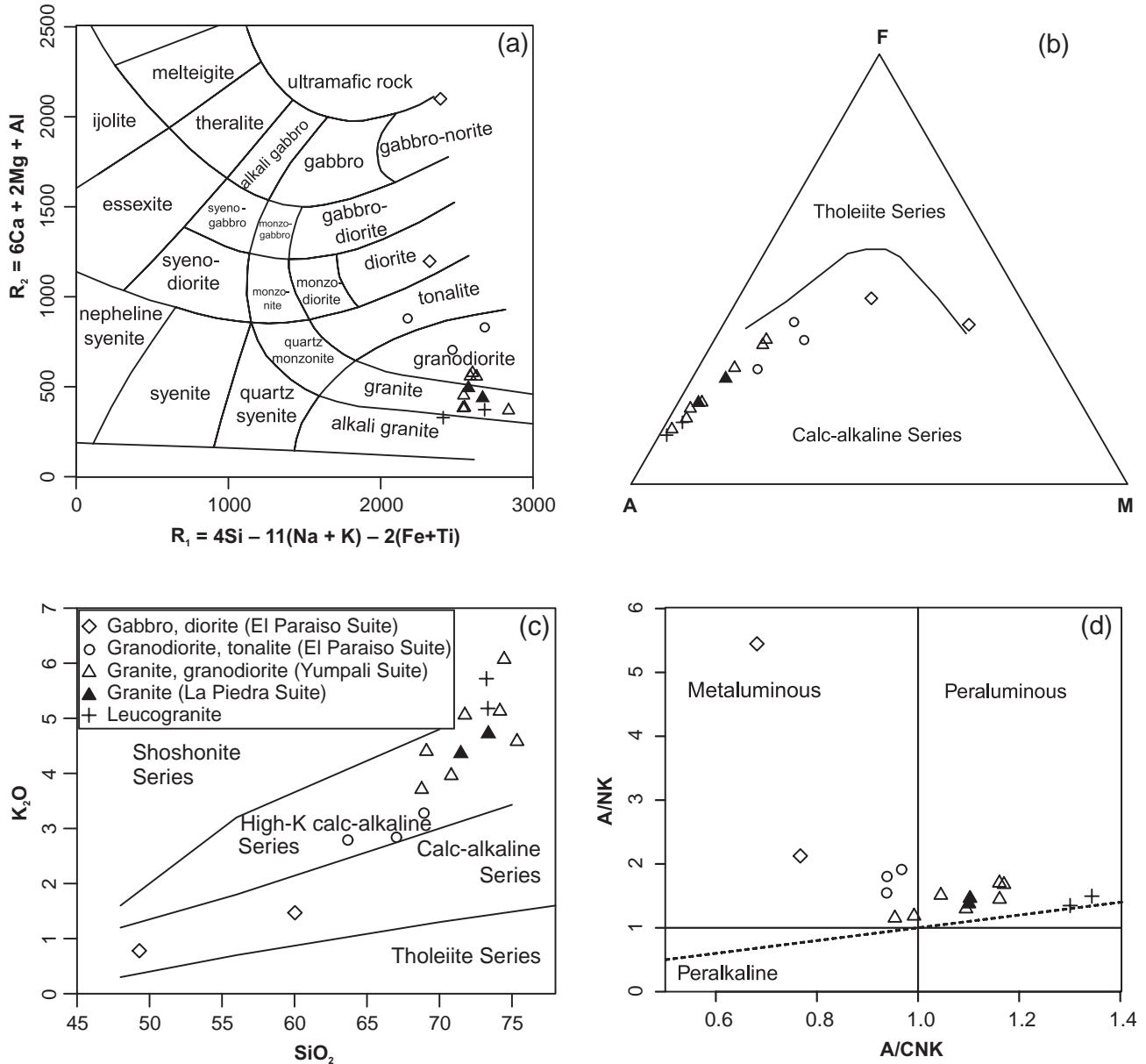


Fig. 5 Chemical composition of the plutonic rocks of the Dipilto Batholith. **a** – R_1 vs. R_2 classification diagram (De La Roche et al. 1980); **b** – AFM diagram (A = Na₂O + K₂O, F = FeO + Fe₂O₃, M = MgO, all oxides are in wt. %; Irvine and Baragar 1971); **c** – SiO₂ vs. K₂O plot (Peccerillo and Taylor 1976); **d** – A/CNK vs. A/NK plot (A = Al₂O₃, C = CaO, N = Na₂O, K = K₂O; all oxides are in mol. %; Shand 1943).

Baragar 1971; Fig. 5b) and belong to the shoshonitic or high K-series (Peccerillo and Taylor 1976; Fig. 5c). Binary plots (Fig. 6) display negative correlations of SiO₂ with CaO, FeO_t, and MgO but positive correlations with K₂O and Rb.

Granitoids of the El Paraiso Suite (Tab. 5) are metaluminous (A/CNK = 0.93–0.97; Fig. 5d) with low K₂O/Na₂O (0.8–1.0) and MgO/FeO_t (0.37–0.54) ratios. They are rich in FeO_t, CaO, MgO and Sr (Fig. 6; Tab. 6). The chondrite-normalized REE pattern (Boynton 1984; Fig. 7) of tonalite indicates enrichment in LREE ($La_N/Yb_N = 3.3$) and negative Eu anomaly (Eu/Eu* = 0.7). The chondrite-normalized REE pattern for the dioritic mafic

microgranular enclave is relatively flat ($La_N/Yb_N = 1.0$) with a deep negative Eu anomaly (Eu/Eu* = 0.3). Gabbro is enriched in LREE ($La_N/Yb_N = 4.2$) and shows a positive Eu anomaly (Eu/Eu* = 1.2).

Rocks of the Yumpali (Tab. 5) and La Piedra Suites are subaluminous to slightly peraluminous (A/CNK = 0.95–1.17), with K₂O/Na₂O = 1.3–2.2 and MgO/FeO_t = 0.13–0.32. In comparison with the rocks of the El Paraiso Suite (Fig. 8), they exhibit slight enrichment in K, Ba, Rb, Th, La and Ce. The chondrite-normalized REE patterns (Fig. 6; Tab. 6) of both suites indicate variable enrichment in LREE ($La_N/Yb_N = 3.9–6.6$) and negative Eu anomalies (Eu/Eu* = 0.2–0.5).

Two samples of felsic tourmaline leucogranites (Tab. 5) have high contents of K_2O (5.2–5.7 wt. %), with K_2O/Na_2O ratios of *c.* 1.9 and high A/CNK (1.30–1.34). Leucogranites are enriched in Rb, K and depleted in Sr, Nb, Ta, P, Hf, Zr, and Ti compared with the average upper continental crust (Fig. 8; Taylor and McLennan 1985). These two samples exhibit various values of the fractionation indexes (e.g., TiO_2 , K/Rb). Typical are lower total contents of REE in comparison with granitoids of the Yumpali and La Piedra suites (37–101 vs. 160–211 ppm; Tab. 6). The decrease in Zr, REE and Th abundances from the Yumpali Suite to leucogranite (Fig. 8) is consistent with fractionation of accessory silicates and phosphates (e.g., zircon, monazite). The chondrite-normalized REE patterns of the leucogranites (Fig. 6) exhibit variable LREE fractionation ($La_N/Yb_N = 1.6$ –4.8) and negative Eu anomalies ($Eu/Eu^* = 0.2$ –0.5).

Zircon saturation temperatures (Watson and Harrison 1983; Tab. 2) calculated for the El Paraiso, Yumpali and La Piedra suites (743–843 °C) are higher than those obtained from the leucogranites (653–739 °C). This difference can be interpreted as an evidence for a higher degree of leucogranites fractionation (Hoskin et al. 2000).

6. Textural and paragenetic types and chemical composition of tourmaline

Electron microprobe analyses (Tab. 4) revealed predominantly schorl–foitite tourmalines in the granitoids of the Dipilto Batholith ($X_{Fe} = 0.53$ –0.98, $Na = 0.21$ –0.77 apfu). High con-

tents of Al_{tot} (≤ 7.04 apfu) and F (≤ 0.46 apfu) indicate the predominance of “oxy-foitite”, oxy-schorl and fluor-schorl components. All the microprobe analyses display low concentrations of Ti (≤ 0.17 apfu), Ca (≤ 0.13 apfu), K (≤ 0.02 apfu) and Mn (≤ 0.04 apfu). Five types of tourmaline were distinguished in the granitoids of the Dipilto Batholith and its contact aureole.

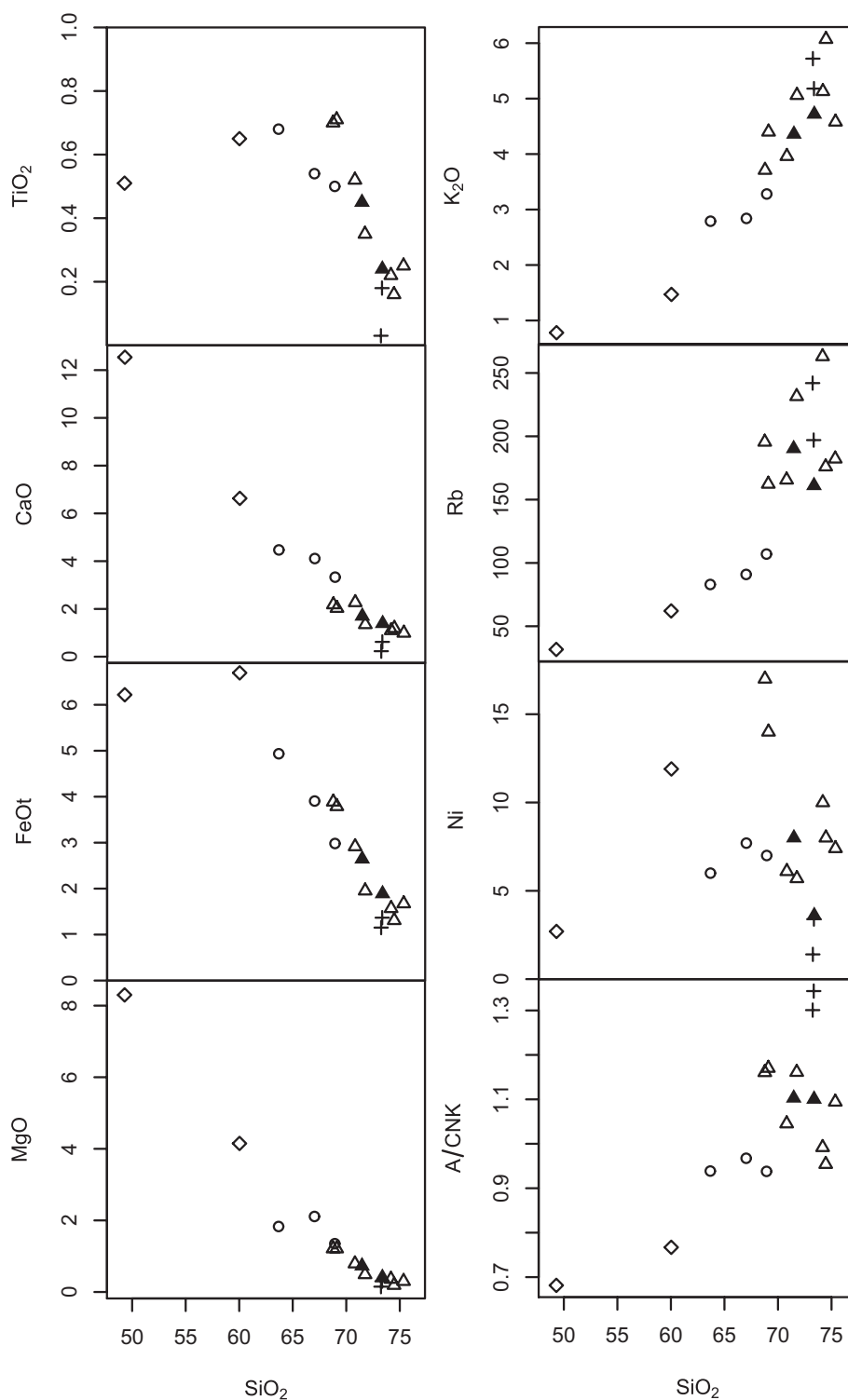


Fig. 6 Variation diagrams of silica versus selected major-element oxides (wt. %) or trace elements (ppm) in magmatic rocks of the Dipilto Batholith (same symbols as in Fig. 5).

Tab. 6 Trace-element analyses of representative rocks from the Dipilto Batholith (in ppm)

Sample	D008	D012	D071	H045	D064	D071/C	H046	H022	H056/A
Ba	855	711	1048	628	671	675	96	155	555
Co	2.7	4.6	7.6	2.4	4.3	1.0	0.9	24.7	8.8
Cu	3.3	6.6	20.2	2.0	8.0	3.1	1.6	10.0	2.0
Ni	5.7	6.1	14.0	3.6	8.0	3.4	1.4	2.7	7.7
Rb	231.5	165.6	162.3	161.1	190.3	197.0	242.0	31.7	90.9
Sr	83.9	124.0	155.9	101.1	114.1	84.8	19.8	497.5	226.3
V	23	32	69	14	32	9	8	247	62
Sn	9	5	4	4	6	5	7	2	3
Zn	47	67	64	34	53	2	4	12	49
As	4.5	5.3	5.0	1.4	2.8	0.6	<0.5	1.6	4.7
U	5.4	3.5	3.2	2.6	6.9	3.1	1.3	0.8	4.6
Nb	16.5	17.0	14.3	7.8	15.2	12.4	3.1	2.3	8.7
Mo	0.3	0.8	1.2	0.1	0.4	0.4	0.1	0.3	0.7
Y	47.0	40.1	46.1	49.4	48.0	26.7	18.5	11.1	23.3
Zr	193.4	245.9	270.8	122.0	220.1	68.5	21.9	60.3	173.9
Pb	3.9	4.1	3.5	3.7	3.3	6.6	4.7	1.7	3.2
Cd	<0.1	<0.1	<0.1	0.1	0.2	<0.1	<0.1	0.1	0.1
Cs	14.0	6.0	6.8	8.6	13.9	7.0	5.8	2.6	4.4
Th	18.8	14.9	15.0	11.6	13.0	7.7	4.3	2.3	9.4
Ta	1.6	1.3	0.8	0.7	1.6	1.5	0.7	0.1	0.7
Hf	6.1	6.9	7.9	3.8	6.6	2.2	1.1	1.7	5.4
Sc	7	10	12	7	9	7	6	41	15
Au	1.9	6.9	0.9	15.1	13.1	1.0	0.6	2.0	0.9
Sb	<0.1	<0.1	<0.1	<0.1	<0.1	<0.1	<0.1	<0.1	<0.1
Ag	<0.1	<0.1	<0.1	<0.1	<0.1	0.2	<0.1	<0.1	<0.1
Hg	<0.01	<0.01	<0.01	<0.01	<0.01	<0.01	<0.01	<0.01	<0.01
Tl	0.6	0.6	0.6	0.4	0.7	0.1	0.1	0.1	0.2
Bi	<0.1	0.2	0.1	<0.1	0.2	5.7	<0.1	<0.1	<0.1
W	0.7	<0.5	1.3	<0.5	0.8	0.8	1.1	<0.5	<0.5
Ga	15.8	17.4	16.7	15.3	17.3	17.0	21.1	15.6	15.1
Se	<0.5	0.6	<0.5	<0.5	<0.5	<0.5	<0.5	<0.5	<0.5
La	39.8	38.5	35.1	27.2	27.9	18.4	5.0	7.0	12.7
Ce	83.2	82.9	76.4	62.1	60.0	38.6	9.5	15.4	28.7
Pr	10.77	9.97	9.63	7.66	7.51	4.87	1.65	2.09	3.71
Nd	39.8	38.1	37.8	30.7	29.5	18.4	6.9	9.5	15.7
Sm	8.22	7.42	7.97	6.86	6.40	3.95	2.31	2.14	3.70
Eu	0.76	0.88	1.10	0.72	0.83	0.63	0.17	0.82	0.87
Gd	7.73	6.64	7.56	7.12	6.69	3.93	2.60	2.13	3.73
Tb	1.41	1.20	1.38	1.36	1.27	0.74	0.59	0.36	0.67
Dy	8.03	6.64	7.82	8.03	7.58	4.36	3.31	2.00	3.81
Ho	1.60	1.36	1.56	1.72	1.56	0.87	0.65	0.40	0.82
Er	4.40	3.99	4.52	4.96	4.67	2.52	1.88	1.16	2.46
Tm	0.69	0.63	0.68	0.75	0.78	0.40	0.32	0.17	0.41
Yb	4.37	3.91	4.16	4.49	4.81	2.61	2.16	1.13	2.59
Lu	0.63	0.57	0.61	0.66	0.70	0.38	0.31	0.16	0.41
Be	2	2	2	2	2	1	2	1	1

6.1. Tourmaline nodules in granites of the Yumpali Suite (type I)

Tourmaline nodules are often concentrated at the contact of the Yumpali Suite granitoids with metamorphic rock and granodiorites–tonalites of the El Paraiso Suite. Anhedral to subhedral tourmaline commonly replaces albitic plagioclase and K-feldspar (Figs 8a–b, 9a–b) whereas

oligoclase (An_{27-39}) is less affected and usually preserves euhedral to subhedral crystal shape (Figs 9b, 10a–b). In the central part, nodules are also present as skeletal fan-shaped aggregates of subhedral columns. Tourmaline (Fig. 11a–c) is present as Al-rich schorl (Al = 6.22–6.59 apfu, $X_{Fe} = 0.72-0.83$, Na = 0.58–0.72 apfu) with relatively low contents of F (0.05–0.22 apfu). The grains mostly show chemically inhomogeneous cores with

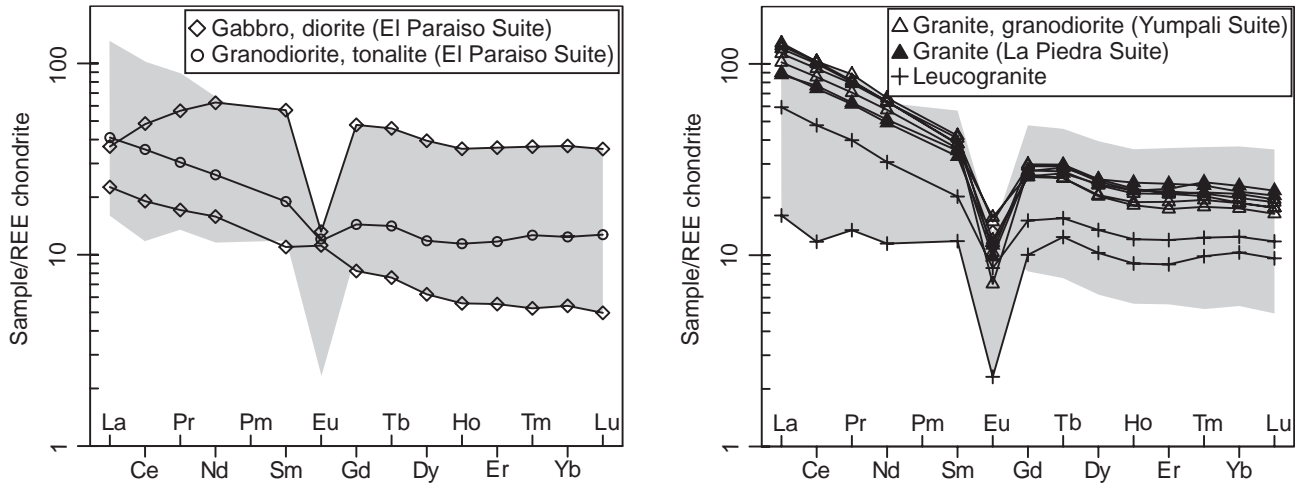


Fig. 7 Chondrite-normalized (Boynnton 1984) REE diagrams. Grey areas represent the fields obtained for all studied rocks from Dipilto Batholith.

smooth zoning (Fe = 1.69–1.90 apfu) rimmed by a zone with higher Fe content (2.08–2.10 apfu). The decrease in Al and increase in Fe + Mg with constant Na contents in the central part of the grains (Fig. 11b) indicate the substitution ${}^Y(\text{Fe} + \text{Mg})_1^{\text{W}}(\text{OH})_1 {}^Y\text{Al}_{-1}^{\text{W}}\text{O}_{-1}$. The rim composition of the tourmaline grains evolves towards more Al-rich and Na-deficient compositions with a dominant foitite substitution of ${}^X\text{Al}_1^{\text{W}}\text{OH}_1 {}^X\text{Na}_{-1} {}^Y(\text{Fe} + \text{Mg})_2^+ {}^Y\text{F}_{-1}$ (Fig. 12a).

6.2. Tourmaline in the leucogranite dykes (type II)

Tourmaline in the leucogranite dykes is present as disseminated subhedral columns up to 1 cm long or as anhedral grains inside small tourmaline nodules (up to 2 cm in diameter, Fig. 3d). It displays higher contents of Al (6.60–6.87 apfu), range of X_{Fe} (0.53–0.90) and Na (0.33–0.60 apfu) and lower content of F (0.00–0.16 apfu; Fig. 12b–c) compared with the type I. Disseminated grains are usually relatively homogeneous (Fe = 1.53–1.84 apfu) in contrast to tourmalines in nodules (Fig. 12d; Fe = 1.19–1.86 apfu). The decrease in the Al

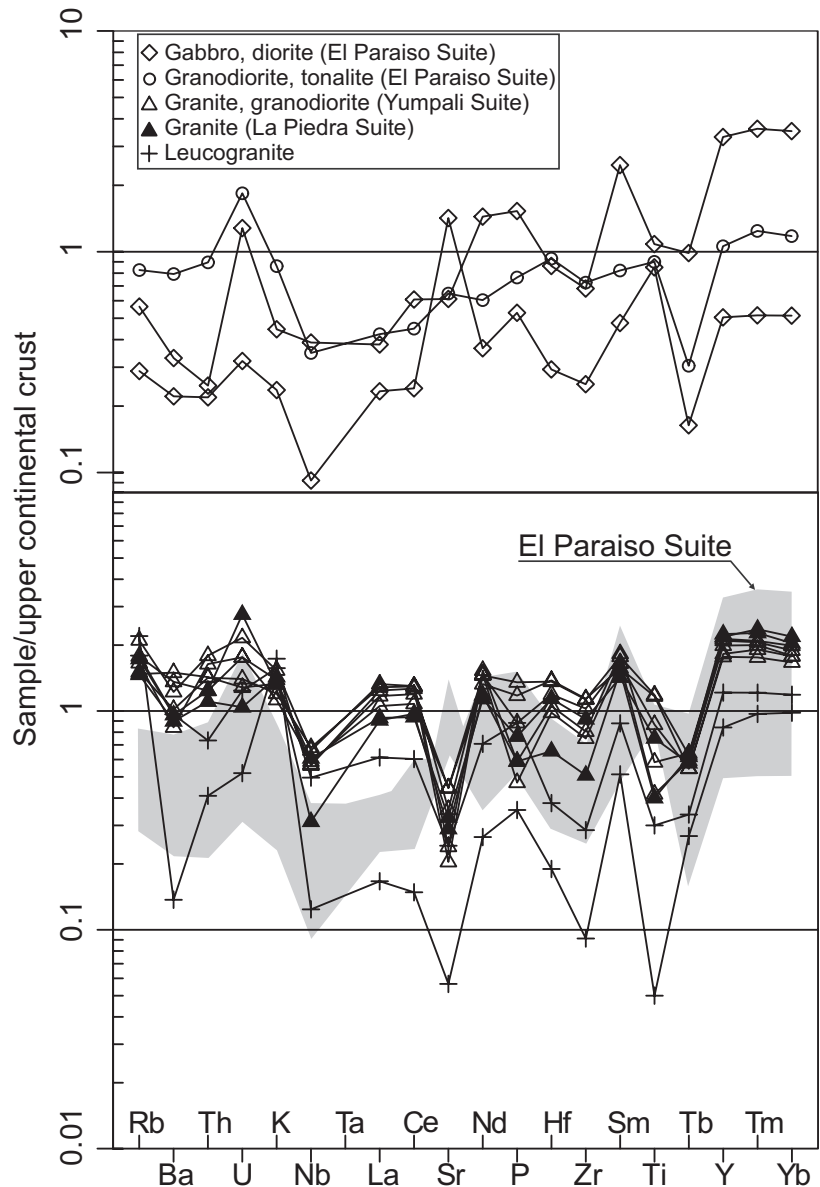


Fig. 8 Comparison of trace-element contents in metaluminous (El Paraiso Suite) and peraluminous (granites to granodiorites of the Yumpali Suite, granites of the La Piedra Suite and leucogranites) rocks of the Dipilto Batholith in spider plots (normalized by the upper continental crust according to Taylor and McLennan 1985).

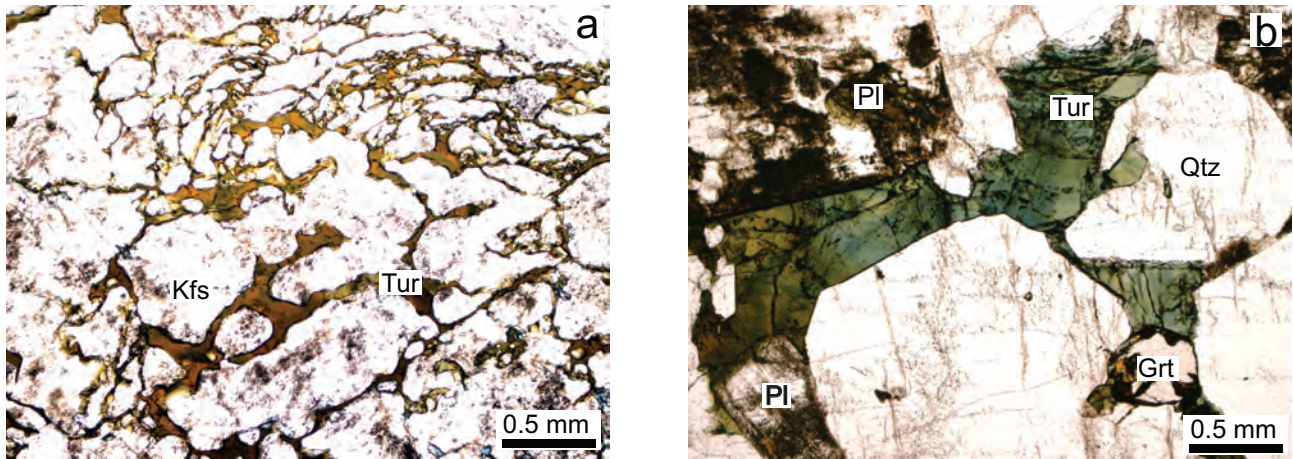


Fig. 9 Photomicrographs of tourmaline (plane polarised light). **a** – Tourmaline preferably replacing albite perthites in K-feldspar phenocrysts from tourmaline nodule in the Yumpali Suite granite (D095); **b** – Tourmaline partially replacing mainly K-feldspar in the nodule from leucogranite dyke (D046); in contrast, plagioclase, quartz and garnet preserve euhedral to subhedral crystal shapes.

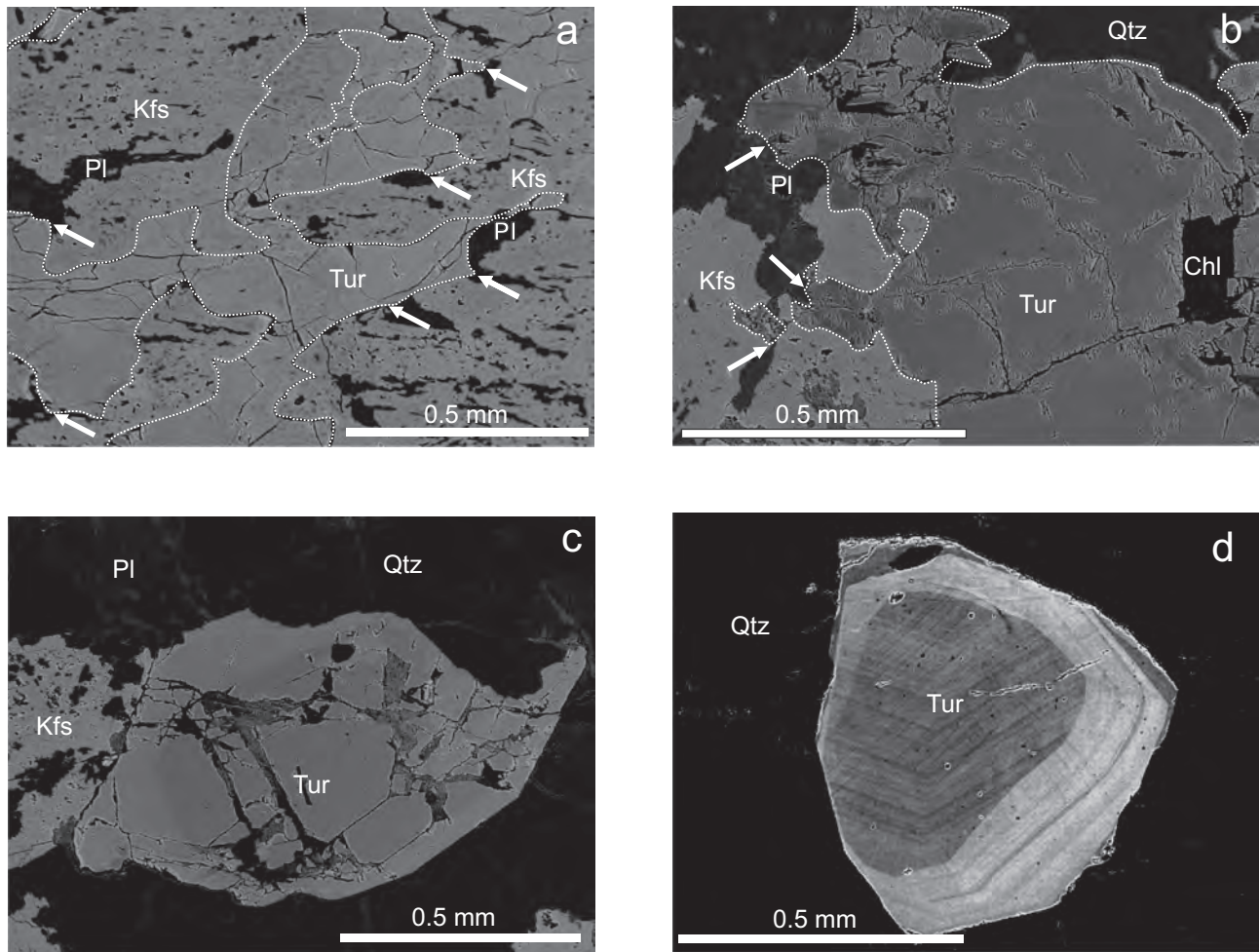


Fig. 10 Back-scattered electron (BSE) images of tourmaline. **a** – Tourmaline partially replacing perthites and K-feldspar in nodules in the granite of the Yumpali Suite (D095); **b** – Tourmaline partially replacing plagioclase in the small nodule from leucogranite dyke (D071C); **c** – Disseminated tourmaline in pegmatite (D041); **d** – Euhedral oscillatory-zoned tourmaline from a quartz vein (D034). In Fig. 10a–b, the arrows indicate replacement of feldspars by tourmaline (original tourmaline outlines are marked by white dotted lines).

and Na contents and increase in Fe + Mg (Figs 10–11) is related to foitite substitution ${}^x\text{Ca}_1{}^y\text{Al}_1{}^x\text{Na}_{-1}{}^y(\text{Fe} + \text{Mg})^{2-}{}_{-1}$ coupled with the substitution of Fe for Mg (Mg Fe_{-1}) (Fig. 12d).

6.3. Tourmaline of pegmatite dykes (type III)

Pegmatite dykes contain euhedral or subhedral grains of disseminated tourmaline, up to 2 cm long (Fig. 3e). It usu-

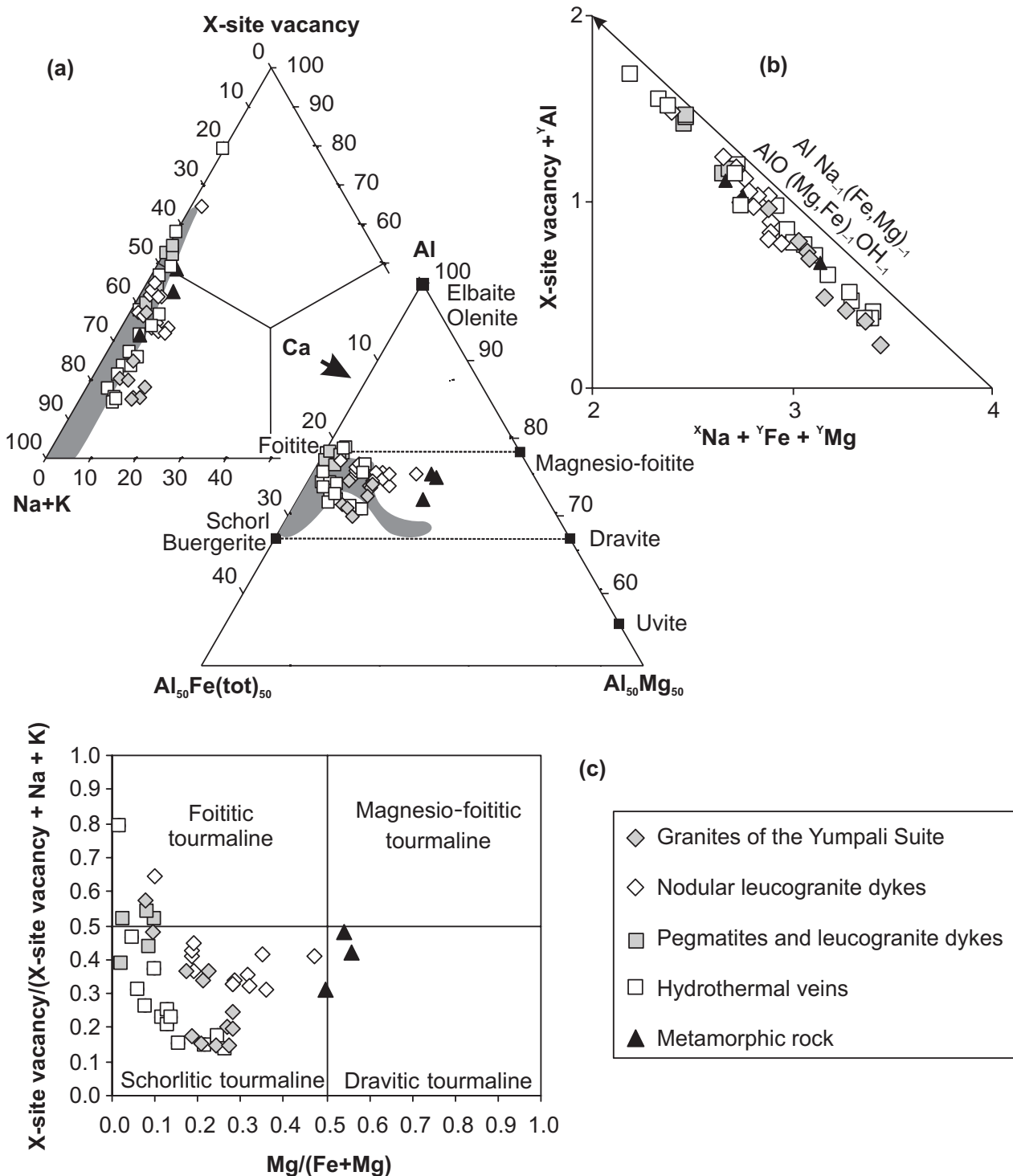


Fig. 11 Classification diagrams for the tourmaline group minerals. **a** – Ternary Na (K)–X-site-vacancy–Ca and $\text{Al}_{50}\text{Fe}_{50}$ –Al– $\text{Al}_{50}\text{Mg}_{50}$ plots after Hawthorne and Henry (1999). Dark grey area represents chemical composition tourmaline from F-rich granite systems (Sinclair and Richardson 1992; Buriánek and Novák 2007; Kubiš and Broska 2010); **b** – Diagram ${}^x\text{Na} + {}^y\text{Fe} + {}^y\text{Mg}$ vs. X-site-vacancy + ${}^y\text{Al}$ and **c** – $\text{Mg}/(\text{Mg} + \text{Fe})$ vs. X-site-vacancy / (X-site-vacancy + Na + K) plots after Henry et al. (2011).

ally exhibits simple zoning (Fig. 10c) with a foitite-rich core (Al = 6.94–7.04 apfu, $X_{\text{Fe}} = 0.90\text{--}0.98$, F = 0.00–0.12 apfu, Na = 0.44–0.57 apfu), and a thin schorl rim (Al = 6.86–6.91 apfu, $X_{\text{Fe}} = 0.91\text{--}0.98$, F = 0.05–0.10 apfu, Na = 0.53–0.57 apfu). Tourmaline grains evolve towards more Na-rich and Al-deficient compositions with predominant substitution of ${}^{\text{X}}\text{Na}_1{}^{\text{Y}}(\text{Fe} + \text{Mg})_2{}^{\text{Z}}\text{Al}_{-1}$ (Fig. 12a).

6.4. Tourmaline of quartz veins (type IV)

Quartz veins, 1 to 50 mm thick, having sharp contacts with the metamorphic rocks and granitoids, locally contain small cavities or pockets with columnar to needle-like crystals of tourmaline (Fig. 3f). Tourmaline often partly replaces plagioclase and K-feldspars of the surrounding granites of the Yumpali Suite. Sometimes, hydrothermal quartz with tourmaline crystals partly fills the miarolitic cavities in the pegmatites. Tourmaline (Al =

6.26–6.83 apfu, $X_{\text{Fe}} = 0.73\text{--}0.95$, F = 0.23–0.46 apfu, Na = 0.51–0.77 apfu) displays oscillatory zoning (Fig. 10d). An increase in F and Na towards rim (Na = 0.58–0.60 apfu) and no systematic variations in Al, Fe and Mg were observed (Fig. 11b–c). Thin younger foitite rims are very rare (Al = 6.89–6.98 apfu, $X_{\text{Fe}} = 0.92\text{--}0.98$, F = 0.00 apfu, Na = 0.21–0.43 apfu). The main substitution trend related to the increase in Na and Mg + Fe²⁺ and decrease in Al and the X-site vacancy corresponds well to the substitution ${}^{\text{X}}\text{Na}_1{}^{\text{Y}}(\text{Fe} + \text{Mg})_2{}^{\text{W}}(\text{OH})_1{}^{\text{X}}\text{Al}_{-1}{}^{\text{W}}\text{O}_{-1}$ (oxy-schorl type substitution; Figs 10b–c, 11a) and/or ${}^{\text{X}}\text{Na}_1{}^{\text{Y}}\text{Al}_1{}^{\text{W}}\text{OH}_1{}^{\text{X}}\text{Na}_{-1}{}^{\text{Y}}(\text{Fe} + \text{Mg})_2{}^{\text{Z}}\text{F}_{-1}$ (Fig. 12b–c).

6.5. Tourmaline in the contact metamorphic aureole (type V)

Accessory tourmaline is also present in the andalusite-cordierite schist in the contact aureole of the Dipilto

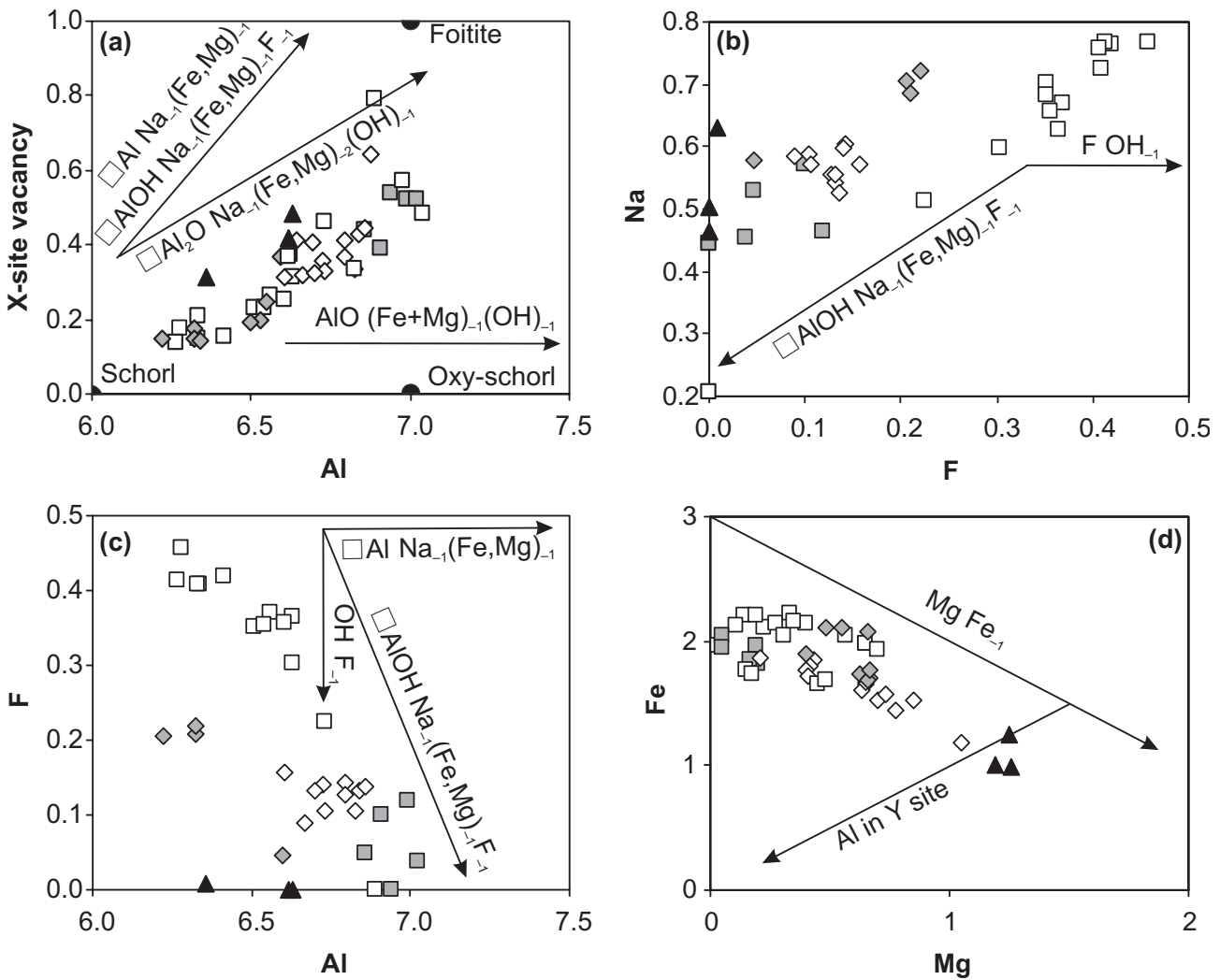


Fig. 12 Diagrams illustrating substitution mechanisms in the tourmaline group minerals. **a** – Al vs. X-site vacancy; **b** – F vs. Na; **c** – Al vs. F; **d** – Mg vs. Fe (same symbols as in Fig. 11).

Batholith. Columnar crystals have alignment following the foliation and correspond to dravite ($\text{Al} = 6.35\text{--}6.63$ apfu, $X_{\text{Fe}} = 0.50\text{--}0.44$, $F = 0.00\text{--}0.01$ apfu, $\text{Na} = 0.46\text{--}0.63$ apfu).

7. Discussion

7.1. Magmatic evolution of the Dipilto Batholith

The estimated P–T conditions in the contact aureole of the Dipilto Batholith ($500\text{--}650^\circ\text{C}$ and ~ 0.2 GPa) as well as those calculated for the rocks of the El Paraiso Suite ($630\text{--}730^\circ\text{C}$ and $0.1\text{--}0.2$ GPa) indicate emplacement at a relatively shallow crustal level (*c.* 6 km; Buriánek and Dolníček 2011).

The Cretaceous Dipilto Batholith represents a petrographically and chemically heterogeneous granitoid body, which consists principally of four distinct suites of magmatic rocks (Tab. 2). The El Paraiso Suite tonalites–granodiorites are metaluminous whereas Yumpali Suite is subaluminous to slightly peraluminous, and La Piedra Suite with leucogranitic dykes are strongly peraluminous. This petrographical variability is typical of calc-alkaline intrusions with a crustal–subcrustal hybrid origin (Castro et al. 1991).

The El Paraiso Suite displays evidence of magma mixing and mingling of the crustal melt with the mantle-derived, basic magma. In terms of major- and trace- element compositions, the El Paraiso Suite plots systematically between the gabbro and the S-type granites of the Yumpali Suite. Textural evidence for magma mixing (e.g., Sparks et al. 1977; Gamble 1979; Hibbard 1991; Janoušek et al. 2004; Slaby and Martin 2008) is documented in plagioclase and mafic microgranular enclaves. More calcic, partially resorbed, weakly zoned cores ($\text{An}_{43\text{--}45}$) are preserved in most of the oscillatory-zoned andesine phenocrysts ($\text{An}_{32\text{--}41}$) in the tonalite and mafic microgranular enclaves. These cores are interpreted as relics of xenocrysts from a more mafic rock entrapped by the tonalitic magma due to magma mixing (Hibbard 1981; Turner and Campbell 1986; Hess 1989; Barbarin 1990; Janoušek et al. 2000; Castro 2001; Janoušek et al. 2004). Magma mixing and mingling are also documented for cordierite-bearing granodiorites of the Yumpali Suite by the geochemistry (e.g., relative high content of Ni; Fig. 6) and petrography (presence of small biotite-rich mafic microgranular enclaves close to the gradual contact with El Paraiso Suite tonalite).

The chemical composition and mineralogy (e.g., cordierite, muscovite) indicate typically S-type signatures for granites of the Yumpali and La Piedra suites. Cordierite-rich xenoliths are richer in Al-minerals (e.g., sillimanite,

hercynite) and these rocks exhibit metamorphic textures typical of the restites from partial melting of the crustal rocks (e.g., Barbey 1991).

The variations in the Rb, K_2O , CaO, FeO, MgO , TiO_2 and REE contents in the granitoids of the Yumpali and La Piedra suites suggest that the plagioclase, K-feldspar and biotite fractionation (probably together with ilmenite, accessory silicates and phosphates) played a significant role in the evolution of these rocks. The majority of the granites with high Rb/Sr ratios can be modelled by removing large proportions of a cumulate dominated by plagioclase and K-feldspar from the cordierite–biotite granite sample (D071, Fig. 13a). Whole compositional spectrum could have been derived by up to 45% fractional crystallization

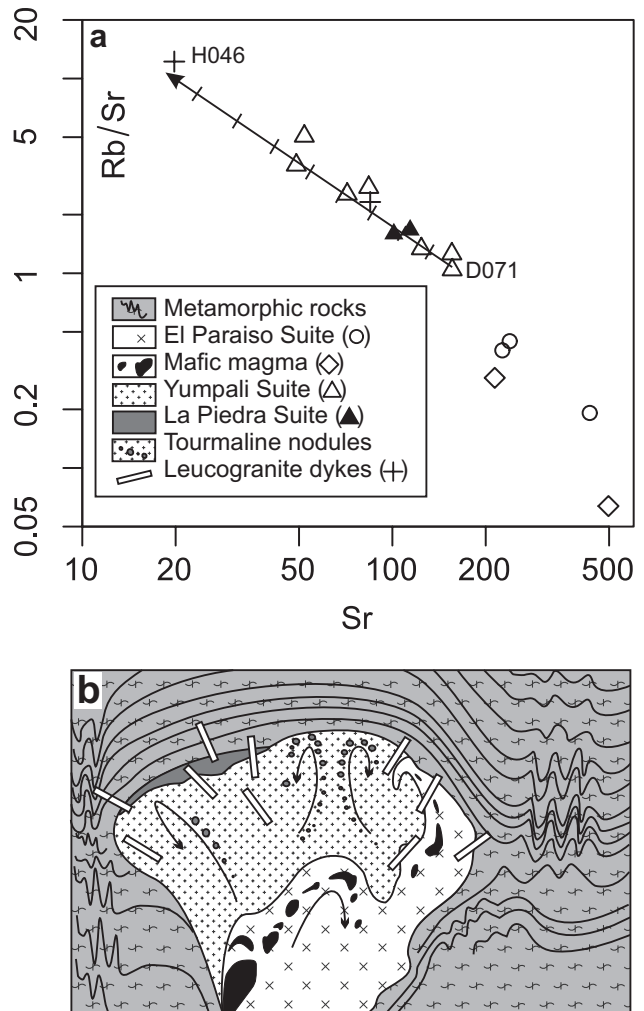


Fig. 13 Magmatic evolution of the Dipilto Batholith. **a** – Diagram of $\log(\text{Sr})$ vs. $\log(\text{Rb/Sr})$ with fractional crystallization trend for peraluminous rocks of the Dipilto Batholith. Solid line with crosses corresponds to increments of 5% fractional crystallization. Whole compositional spectrum could have been derived by up to 45% fractional crystallization of plagioclase (55 wt. %), K-feldspar (40 wt. %) and biotite (5 wt. %). **b** – Schematic model for the emplacement of the Dipilto Batholith, showing relationship between main rock types. Arrows indicate the possible direction of magma flow.

of plagioclase (55 wt. %), K-feldspar (40 wt. %) and biotite (5 wt. %).

7.2. Chemical compositions of biotite and tourmaline as indicators of the evolution of the granitoids from the Dipilto Batholith

Biotite (Tab. 3) is the most common rock-forming constituent in all granitoids of the Dipilto Batholith and can be used to distinguish between individual suites. Biotite from metaluminous rocks of the El Paraiso Suite exhibits relatively low X_{Fe} (Fe/(Fe + Mg)) and $^{\text{IV}}\text{Al}$ values compared with biotite in peraluminous granites of the Yumpali and La Piedra suites (Fig. 4a). Biotite from granites of the latter two suites mostly has higher F contents (0.08–0.13 apfu) than that in the other studied granitoids (tonalite 0.00 apfu, tourmaline granite 0.04–0.09 apfu; Fig. 4b). Biotite has a strong tendency to recrystallize and the F values in the biotite are not a good monitor of F in the melts (Icenhower and London 1995). However, the relatively low F contents in the biotite from all studied peraluminous granites indicate that Dipilto Batholith represents a F-poor granitic system. Igneous biotite continuously equilibrates with its host melt (Barbarin 2005) and thus can be used to monitor its evolution. Biotite in tourmaline granite dykes exhibits higher X_{Fe} values compared with peraluminous granites of the Yumpali and La Piedra suites (Fig. 4a). Increase in the biotite X_{Fe} indicates progressive fractionation of the peraluminous melt (e.g., Villaseca and Barbero 1994) during final stages of the Dipilto Batholith formation.

Scarce appearance of **tourmaline** (Tab. 4) in dominant peraluminous granites of the Yumpali and La Piedra suites (tourmaline nodules, type I) and common occurrence of magmatic and/or hydrothermal tourmaline in pegmatite, leucogranite dykes and quartz–tourmaline veins (types II–IV), provide evidence for the formation of this mineral mainly during the late-magmatic to subsolidus evolutionary stages of the peraluminous granites in the Dipilto Batholith. Schorlitic tourmaline I is rimmed by foititic tourmaline (Fig. 11c) with low contents of F, reflecting the hydrothermal stage of evolution of the tourmaline nodules (e.g., Henry et al. 2002). Compared with schorlitic tourmaline from the nodules (I), the tourmaline from leucogranite dykes (II) exhibits lower contents of Na and F and higher Al. Tourmalines III from pegmatite dykes have similar or lower contents of Na and F than tourmalines from the leucogranite dykes (II). Their higher X_{Fe} indicates a growth from a more fractionated granitic melt (e.g., Buriánek and Novák 2007). The chemical composition of the tourmalines from the quartz veins (IV) with high contents of Fe, F and Na points to crystallization from highly fractionated hydrothermal fluids (Henry and Dutrow 2011).

Chemical composition of tourmaline evolved from Mg-rich schorl (rare foitite) in peraluminous granite nodules, through schorl–foitite in the pegmatite to F-rich schorl–foitite in the hydrothermal veins (Fig. 11a–c). This evolutionary trend is different from other F-rich granite systems (Fig. 11a) previously published from many localities (Sinclair and Richardson 1992; Buriánek and Novák 2007; Kubiš and Broska 2010).

7.3. Evolution of boron-rich melt in the Dipilto Batholith

Rare tourmaline is present in the peraluminous granitoids of the Yumpali Suite and common in the younger leucogranites, pegmatites and quartz dykes spatially and genetically related to the Yumpali Suite. The distribution of tourmaline suggests that the parental peraluminous melt was boron-undersaturated during most of its crystallization because the majority of the granites and granodiorites of the Yumpali Suite are tourmaline-free. At the same time, the activities of B, Al, Fe, Mg and Ti are essential in controlling the formation and separation of the boron-rich granitic melt (e.g., Pesquera et al. 2013). For example crystallization of tourmaline in peraluminous granite requires a high content of boron (1–4 wt. % B_2O_3 in melt at ~750 °C, Wolf and London 1997).

Formation of tourmaline nodules marked the initial stages of the boron saturation from melts during the crystallization of peraluminous granites of the Yumpali Suite. Boron enrichment caused depolymerization of the some domains in the parental melt and decreased its density, viscosity, liquidus and solidus temperatures (London et al. 1996; Wolf and London 1997; Kubiš and Broska 2005). Hence tourmaline nodules grew from bubbles of such an immiscible volatile-rich melt (e.g., Veksler and Thomas 2002; Veksler et al. 2002; Thomas et al. 2003; Veksler 2004, Balen and Petrinec 2011). Tourmaline in the central part of the nodules sometimes forms fan-shaped aggregates, which are typical of magmatic crystallization (Perugini and Poli 2007). However, tourmaline partially replaced rock-forming minerals (e.g., plagioclases and albitic perthites in the K-feldspar; Figs 8a–b, 9a) in the external part of the nodules. These features indicate the formation of tourmaline under a wide range of conditions from late magmatic crystallization to the subsolidus stage (see e.g., Sinclair and Richardson 1992; Buriánek and Novák 2004; Trumbull et al 2007; Balen and Broska 2011; Balen and Petrinec 2011).

Tourmaline nodules are often concentrated in the narrow zones in granitoids of the Yumpali Suite that are approximately perpendicular to the contact with the metamorphic aureole. Such a spatial distribution of the nodules may be related to the thermal contrast (Johannes and Holtz 1996) between the cooler, fluid-rich

peraluminous granitic melt of the Yumpali Suite (Fig. 13b) and the more mafic melt of the El Paraiso Suite with higher solidus temperature (Wyllie 1977; Schmidt and Thompson 1996). Magma convection caused by this thermal gradient perhaps resulted in movement of bubbles of overheated peraluminous water- and/or boron-rich melts forming spheres in order to decrease surface tension (Shinohara and Hedenquist 1997). These individual bubbles buoyantly rose to the top of the magma body. The low viscosity and density of the B-rich hydrous melt enhanced the mobility in the highly polymerized dominant peraluminous melt and the formation of narrow zones of tourmaline nodules (Trumbull et al 2007; Balen and Petrinec 2011).

Second stage of boron saturation was related to formation of fluid-rich residual melt. The younger pegmatite and leucogranite dykes represented final-stage fractional crystallization of the Yumpali Suite peraluminous granites. Two studied leucogranites exhibit different degrees of magmatic fractionation (Figs 6, 12a). The sample of evolved leucogranite contains the lowest TiO₂ (0.03 wt. %), Sr (20 ppm) and Ba (96 ppm) contents in the dataset; in contrast, the second sample has the same composition as the host granites of the Yumpali Suite. Wide range of tourmaline chemical compositions (e.g., X_{Fe} = 0.53–0.98) also indicates a variable degree of magmatic fractionation in leucogranite and pegmatite dykes.

Subsequently, fluorine-rich schorl to foitite in quartz veins crystallized from B- and F-rich hydrothermal fluids. On the other hand, euhedral tourmaline in coarse-grained pegmatite grew directly from the residual boron-rich melt, together with other rock-forming minerals (e.g., feldspars or biotite) and is relatively F-poor. These differences between the hydrothermal and magmatic tourmaline probably reflected the distribution of F between the micas (Fig. 4b) and the tourmaline in the pegmatite, because the experimental data show that the F is concentrated in the granitic melt relative to the coexisting fluid (Xiaolin et al. 1998).

8. Conclusions

The Cretaceous Dipilto Batholith is composed of four main suites: (1) biotite and amphibole–biotite granodiorites to tonalites (El Paraiso Suite), (2) porphyritic biotite granites to granodiorites sometimes with cordierite and/or tourmaline (Yumpali Suite), (3) medium-grained biotite to muscovite granites (La Piedra Suite), (4) leucogranites and pegmatites. The petrographic and geochemical features suggest that the parental magmas of the El Paraiso and Yumpali suites were emplaced simultaneously. Textural and chemical data provide evidence for magma-mixing processes mainly in the El Paraiso Suite. Granites

La Piedra and Yumpali suites together with dykes of leucogranites and pegmatites represent typical products of a fractional crystallization of crustally derived melts.

The distribution of tourmaline nodules in the prevailing cordierite–biotite to biotite granites was strongly affected by magma convection triggered by the thermal contrast between the granitoids of the Yumpali and El Paraiso suites. Tourmaline in nodules grew under conditions transitional between those of the boron-rich melt and hydrothermal fluids; it partially replaces the early-crystallized feldspars. Individual nodules are interpreted as pockets of boron-rich melt without significant magmatic fractionation. In contrast, the dykes of pegmatites and leucogranites are a result of variable degrees of the granitic melt fractionation.

Evolution of the tourmaline chemical composition reflects crystallization from melt and fluids generated in the F-poor granite system. The wide compositional range is most consistent with substitutions represented by ${}^x\text{Al}_1{}^y\text{Al}_1{}^z\text{Na}_{-1}{}^w(\text{Fe} + \text{Mg})^{2+}_{-1}$, ${}^x\text{Al}_2{}^y\text{Al}_1{}^z\text{Na}_{-1}{}^w(\text{Fe} + \text{Mg})^{2+}_{-2}{}^w(\text{OH})_{-1}$, Mg Fe_{-1} and ${}^x\text{Al}_1{}^y\text{Al}_1{}^z\text{Na}_{-1}{}^w(\text{Fe} + \text{Mg})^{2+}_{-1}{}^y\text{F}_{-1}$.

The described tourmaline samples record at least two stages of B-rich melt formation during the crystallization of the peraluminous granites of the Dipilto Batholith. The first stage corresponded to crystallization of tourmaline nodules in the cordierite–biotite to biotite granites of the Yumpali Suite. Tourmalines in this closed system evolved from Mg-rich schorl to foitite. Relatively variable F, Al, X_{Fe} (0.72–0.83) contents are typical.

Second stage of boron-rich melts formation represented leucogranite and pegmatite dykes as the product of Yumpali and La Piedra suites fractional crystallization. Increasing degrees of residual melt fractionation are indicated by the chemical composition of leucogranites (e.g., Sr and Ba decrease and Rb increases) and also by the tourmaline chemistry (e.g., X_{Fe} = 0.53–0.90). Disseminated tourmaline (schorl to foitite) in pegmatites, with high X_{Fe} (0.90–0.98), Al (6.86–6.91 apfu) and low F (0.00–0.12 apfu), crystallized during the final magmatic stage.

The second stage magmatic crystallization was terminated by the formation of hydrothermal quartz–tourmaline veins, which filled the cracks in the granites and surrounding metamorphic rocks. Oscillatory-zoned, F-rich schorl to foitite is characterised by variable but usually high X_{Fe} (0.73–0.95) and high F (0.23–0.46 apfu), which increase at the expense of Na. Tourmaline chemical compositions in the pegmatite and hydrothermal veins evolve from schorl through F-rich schorl to foitite. This trend reflects fractionation of the residual granitic melt and subsequent hydrothermal fluids.

Acknowledgements. This work was supported by the Czech Geological Survey, Project No. 321180. The au-

thors wish to thank P. Uher and an anonymous reviewer for critical reviews of the manuscript. M. Štulíková is thanked for revising the English. Last but not least, the careful editorial handling by M. Novák and V. Janoušek helped us to improve the readability of the text.

Electronic supplementary material. Whole-rock geochemical data for granitoids of the Dipilto Batholith from this paper are available online at the Journal web site (<http://dx.doi.org/10.3190/jgeosci.189>).

References

- BALEN D, BROSKA I (2011) Tourmaline nodules: products of devolatilization within the final evolutionary stage of granitic melt? In: SIAL AN, BETTENCOURT JS, DE CAMPOS CP, FERREIRA VP (eds) *Granite-Related Ore Deposits*. Geological Society of London Special Publications 350: 53–68
- BALEN D, PETRINEC Z (2011) Contrasting tourmaline types from peraluminous granites: a case study from Moslavačka Gora (Croatia). *Mineral Petrol* 102: 117–134
- BARBARIN B (1990) Plagioclase xenocrysts and mafic magmatic enclaves in some granitoids of the Sierra Nevada Batholith, California. *J Geophys Res* 95:17747–17756
- BARBARIN B (2005) Mafic magmatic enclaves and mafic rocks associated with some granitoids of the central Sierra Nevada Batholith, California: nature, origin, and relations with the hosts. *Lithos* 80: 155–177
- BARBEY P (1991) Restites in migmatites and autochthonous granites: their main features and their genesis. In: DIDIER J, BARBARIN B (eds) *Enclaves and Granite Petrology*. Elsevier, Amsterdam, pp 479–492
- BOYNTON WV (1984) Cosmochemistry of the rare earth elements: meteorite studies. In: HENDERSON PE (ed) *Rare Earth Element Geochemistry*. Elsevier, Amsterdam, pp 63–114
- BROSKA I, UHER P, LIPKA J (1998) Brown and blue schorl from the Spiš-Gemer granite, Slovakia: composition and genetic relations. *J Czech Geol Soc* 43: 9–16
- BURIÁNEK D, DOLNÍČEK Z (2011) Metamorphic evolution of the contact aureole of the Dipilto Batholith, Eastern Chortis Terrane, Nicaragua. *J Geosci* 56: 9–26
- BURIÁNEK D, NOVÁK M (2004) Morphological and compositional evolution of tourmaline from nodular granite at Lavičky near Velké Meziříčí, Moldanubicum, Czech Republic. *J Czech Geol Soc* 49: 81–90
- BURIÁNEK D, NOVÁK M (2007) Compositional evolution and substitutions in disseminated and nodular tourmaline from leucocratic granites: examples from the Bohemian Massif, Czech Republic. *Lithos* 95: 148–164
- BURIÁNEK D, HRADECKÝ P, HAVLÍČEK P, ČÁP P, NOVOTNÝ R, BALDÍK V (2010) Geological map of Jalapa area 1 : 50 000. Czech Geological Survey, Prague (in Czech)
- CASTRO A (2001) Plagioclase morphologies in assimilation experiments: implications for disequilibrium melting in the generation of granodiorite rocks. *Mineral Petrol* 71: 31–49
- CASTRO A, MORENO-VENTAS I, DE LA ROSA JD (1991) H-type (Hybrid) granitoids: a proposed revision of the granite type classification and nomenclature. *Earth Sci Rev* 31: 237–253
- DE LA ROCHE H, LETERRIER J, GRANDCLAUDE P, MARCHAL M (1980) A classification of volcanic and plutonic rocks using R_1 R_2 -diagram and major element analyses – its relationships with current nomenclature. *Chem Geol* 29: 183–210
- DEMPÍROVÁ L (2010) Evaluation of SiO_2 , Na_2O , MgO , K_2O determinations in silicate samples by z-score obtained from nineteen interlaboratory tests. *Zpr geol Výzk v Roce 2009*: 323–326
- DEMPÍROVÁ L, ŠIKL J, KAŠIČKOVÁ R, ZOULKOVÁ V, KRÍBEK B (2010) The evaluation of precision and relative error of the main components of silicate analyses in Central Laboratory of the Czech Geological Survey. *Zpr geol Výzk v Roce 2009*: 326–330
- DENGO G (1969) Problems of tectonic relations between Central America and the Caribbean. *Trans Gulf Coast Assoc Geol Soc* 19: 311–320
- DINI A, CORRETTI A, INNOCENTI F, ROCCHI S, WESTERMAN DS (2007) Sooty sweat stains or tourmaline spots? The Argonauts at Elba Island (Tuscany) and the spread of Greek trading in the Mediterranean Sea. In: PICCARDI L, MASSE WB (eds) *Myth and Geology*. Geological Society of London Special Publications 273: 227–243
- DONNELLY TW, HORNE GS, FINCH RC, LÓPEZ-RAMOS E (1990) Northern Central America: the Maya and Chortis blocks. In: DENGO G, CASE JE (eds) *The Caribbean Region*. Geological Society of America, Boulder, pp 37–76
- DROOP GTR (1987) A general equation for estimating Fe^{3+} concentrations in ferromagnesian silicates using stoichiometric criteria. *Mineral Mag* 51:431–435
- ERSOY Y, HELVACI C (2010) FC–AFC–FCA and mixing modeler: a Microsoft® Excel® spreadsheet program for modeling geochemical differentiation of magma by crystal fractionation, crustal assimilation and mixing. *Comput Geosci* 36: 383–90
- FIGGE K (1966) Die stratigraphische Stellung der metamorphen Gesteine NW-Nicaraguas. *Neu Jb Geol Paleont, Mh* 4: 193–254 (in German)
- GAMBLE JA (1979) Some relationships between coexisting granitic and basaltic magmas and the genesis of hybrid rocks in the Tertiary central complex of Slieve Gullion, northeast Ireland. *J Volcanol Geotherm Res* 5: 297–316
- HAWTHORNE FC, HENRY DJ (1999) Classification of the minerals of the tourmaline group. *Eur J Mineral* 11: 201–215
- HENRY DJ, DUTROW BL (2011) The incorporation of fluorine in tourmaline: internal crystallographic controls or external environmental influences? *Canad Mineral* 49: 41–56

- HENRY DJ, GUIDOTTI CV (1985) Tourmaline as a petrogenetic indicator mineral: an example from the staurolite-grade metapelites of NW Maine. *Amer Miner* 70: 1–15
- HENRY DJ, DUTROW BL, SELVERSTONE J (2002) Compositional asymmetry in replacement tourmaline – an example from the Tauern Window, Eastern Alps. *Geol Mat Res* 4: 1–18
- HENRY DJ, NOVÁK M, HAWTHORNE FC, ERTL A, DUTROW BL, UHER P, PEZZOTTA F (2011) Nomenclature of the tourmaline-super group minerals. *Amer Miner* 96: 895–913
- HESS PC (1989) *Origins of Igneous Rocks*. Harvard University Press, Cambridge, pp 1–336
- HIBBARD MJ (1981) The magma mixing origin of mantled feldspars. *Contrib Mineral Petrol* 76: 158–170
- HIBBARD MJ (1991) Textural anatomy of twelve magma-mixed granitoid systems. In: DIDIER J, BARBARIN B (eds) *Enclaves and Granite Petrology*. Elsevier, Amsterdam, pp 431–444
- HODGSON G (2000) Introduction to Nicaragua stratigraphic lexicon. Unpublished report, UNAN, Managua, pp 1–184 (in Spanish)
- HOSKIN PWO, KINNY PD, WYBORN D, CHAPPELL BW (2000) Identifying accessory mineral saturation during differentiation in granitoid magmas: an integrated approach. *J Petrol* 41: 1365–1396
- HRADECKÝ P, KYCL P, ŽÁČEK V, HRAZDÍRA P, OPLETAL M, ŠEVČÍK J, ŠEBESTA J (2005) Geological study of the natural hazards in the area Ocotal, province Nueva Segovia, Nicaragua. Unpublished report, Czech Geological Survey, Prague, pp 1–84
- ICENHOWER JP, LONDON D (1995) An experimental study of element partitioning between biotite, muscovite and coexisting peraluminous granitic melt at 200 MPa (H₂O). *Amer Miner* 80: 1229–1251
- IRVINE TN, BARAGAR WRA (1971) A guide to the chemical classification of the common volcanic rocks. *Can J Earth Sci* 8: 523–548
- JANOÚŠEK V, BOWES DR, BRAITHWAITE CJR, ROGERS G (2000) Microstructural and mineralogical evidence for limited involvement of magma mixing in the petrogenesis of a Hercynian high-K calc-alkaline intrusion: the Kozárovec granodiorite, Central Bohemian Pluton, Czech Republic. *Trans Roy Soc Edinb, Earth Sci* 91: 15–26
- JANOÚŠEK V, BRAITHWAITE CJR, BOWES DR, GERDES A (2004) Magma-mixing in the genesis of Hercynian calc-alkaline granitoids: an integrated petrographic and geochemical study of the Sázava intrusion, Central Bohemian Pluton, Czech Republic. *Lithos* 78: 67–99
- JANOÚŠEK V, FARROW CM, ERBAN V (2006) Interpretation of whole-rock geochemical data in igneous geochemistry: introducing Geochemical Data Toolkit (GCDkit). *J Petrol* 47: 1255–1259
- JOHANNES W, HOLTZ F (1996) *Petrogenesis and Experimental Petrology of Granitic Rocks*. Springer Verlag, Berlin, pp 1–335
- KRETZ R (1983) Symbols for rock-forming minerals. *Amer Miner* 68: 277–279
- KUBIŠ M, BROSKA I (2005) Role of boron and fluorine in evolved granitic rock systems (on example Hnilec area, Western Carpathians). *Geol Carpath* 56: 193–204
- KUBIŠ M, BROSKA I (2010) The granite system near Betliar village (Gemeric Superunit, Western Carpathians): evolution of a composite silicic reservoir. *J Geosci* 55: 131–148
- LEAKE BE, WOOLEY AR, ARPS CES, BIRCH WD, GILBERT MC, GRICE JD, HAWTHORNE FC, KATO A, KISCH HJ, KRIVOVICHEV VG (1997) Nomenclature of amphiboles: report of the Subcommittee on Amphiboles of the International Mineralogical Association Commission on New Minerals and Mineral Names. *Canad Mineral* 35: 219–237
- LONDON D (1999) Stability of tourmaline in peraluminous granite systems; the boron cycle from anatexis to hydrothermal aureoles. *Eur J Mineral* 11: 253–262
- LONDON D, MANNING DAC (1995) Chemical variation and significance of tourmaline from southwest England. *Econ Geol* 90: 495–519
- LONDON D, MORGAN GB, WOLF MB (1996) Boron in granitic rocks and their contact aureoles. In: GREW ES, ANOVITZ LM (eds) *Boron: Mineralogy, Petrology and Geochemistry*. Mineralogical Society of America Reviews in Mineralogy and Geochemistry 33: 299–330
- PECCERILLO A, TAYLOR SR (1976) Geochemistry of Eocene calc-alkaline volcanic rocks from the Kastamonu area, northern Turkey. *Contrib Mineral Petrol* 58: 63–81
- PERUGINI D, POLI G (2007) Tourmaline nodules from Capo Bianco aplite (Elba Island, Italy): an example of diffusion limited aggregation growth in a magmatic system. *Contrib Mineral Petrol* 153: 493–508
- PESQUERA A, TORRES-RUIZ J, GARCÍA-CASCO A, GIL-CRESPO PP (2013) Evaluating the controls on tourmaline formation in granitic systems: a case study on peraluminous granites from the Central Iberian Zone (CIZ), Western Spain. *J Petrol* 54: 609–634
- PICHAVANT M, MANNING D (1984) Petrogenesis of tourmaline granites and topaz granites; the contribution of experimental data. *Phys Earth Planet Inter* 35: 31–50
- POUCHOU JL, PICOIR F (1985) „PAP“ (Z) procedure for improved quantitative microanalysis. In: ARMSTRONG JT (ed) *Microbeam Analysis*: 104–106
- RITCHIE AW, FINCH RC (1985) Widespread Jurassic strata on the Chortis Block of the Caribbean Plate. *Geol Soc Am Abstr Progr* 17: 700–701
- ROGERS RD (2003) *Jurassic–Recent Tectonic and Stratigraphic History of the Chortis Block of Honduras and Nicaragua (Northern Central America)*. Unpublished PhD. thesis, University of Texas, Austin, pp 1–289
- ROGERS RD, MANN P, EMMET PA (2007) Tectonic terranes of the Chortis Block based on integration of regional aeromagnetic and geologic data. In: MANN P (ed) *Geologic and Tectonic Development of the Caribbean Plate in*

- northern Central America. Geological Society of America Special Papers 428: 65–88
- SCHMIDT MW, THOMPSON AB (1996) Epidote in calc-alkaline magmas: an experimental study of stability, phase relationships, and the role of epidote in magmatic evolution. *Amer Miner* 81: 462–474
- SHAND SJ (1943) *Eruptive Rocks. Their Genesis, Composition, Classification, and Their Relation to Ore-Deposits with a Chapter on Meteorite*. John Wiley & Sons, New York, pp 1–444
- SHINOHARA H, HEDENQUIST JW (1997) Constraints on magma degassing beneath the Far Southeast porphyry Cu–Au deposit, Philippines. *J Petrol* 38: 1741–1752
- SINCLAIR WD, RICHARDSON JM (1992) Quartz–tourmaline orbicules in the Seagull Batholith, Yukon Territory. *Canad Mineral* 30: 923–935
- SLÁBY E, MARTIN H (2008) Mafic and felsic magma interaction in granites: the Hercynian Karkonosze Pluton (Sudetes, Bohemian Massif). *J Petrol* 49: 353–391
- SPARKS RSJ, SIGURDSSON H, WILSON L (1977) Magma mixing: a mechanism for triggering acid explosive eruptions. *Nature* 267: 315–318
- TAYLOR SR, MCLENNAN SM (1985) *The Continental Crust: Its Composition and Evolution*. Blackwell, Oxford, pp 1–312
- THOMAS R, FÖRSTER HJ, HEINRICH W (2003) The behaviour of boron in a peraluminous granite–pegmatite system and associated hydrothermal solutions: a melt and fluid-inclusion study. *Contrib Mineral Petrol* 144: 457–472
- TRUMBULL RB, KRIENITZ MS, GOTTESMANN B, WIEDENBECK M (2007) Chemical and boron-isotope variations in tourmalines from an S-type granite and its source rocks: the Erongo granite and tourmalinites in the Damara Belt, Namibia. *Contrib Mineral Petrol* 155: 1–18
- TURNER JS, CAMPBELL IH (1986) Convection and mixing in magma chambers. *Earth Sci Rev* 23: 255–352
- VEKSLER IV (2004) Liquid immiscibility and its role at the magmatic–hydrothermal transition: a summary of experimental studies. *Chem Geol* 210: 7–31
- VEKSLER IV, THOMAS R (2002) An experimental study of B-, P- and F-rich synthetic granite pegmatite at 0.1 and 0.2 GPa. *Contrib Mineral Petrol* 143: 673–683
- VEKSLER IV, THOMAS R, SCHMIDT C (2002) Experimental evidence of three coexisting immiscible fluids in synthetic granitic pegmatite. *Amer Miner* 87: 775–779
- VILAND JC, HENRY B, CALIX R, DIAZ C (1996) Late Jurassic deformation in Honduras. Proposals for a revised regional stratigraphy. *J South Am Earth Sci* 9: 153–160
- VILLASECA C, BARBERO L (1994) Chemical variability of Al–Ti–Fe–Mg minerals in peraluminous granitoid rocks from Central Spain. *Eur J Mineral* 6: 691–710
- WATSON EB, HARRISON TM (1983) Zircon saturation revisited: temperature and composition effects in a variety of crustal magma types. *Earth Planet Sci Lett* 64: 295–304
- WILLIAMSON BJ, SPRATT J, ADAMS JT, STANLEY CJ (2000) Geochemical constraints from zoned hydrothermal tourmalines on fluid evolution and Sn mineralization: an example from Fault Breccias at Roche, SW England. *J Petrol* 41: 1439–1453
- WHITNEY DL, EVANS B (2010) Abbreviations for names of rock-forming minerals. *Amer Miner* 95: 185–187
- WOLF MB, LONDON D (1997) Boron in granitic magmas: stability of tourmaline in equilibrium with biotite and cordierite. *Contrib Mineral Petrol* 130: 12–30
- WYLLIE PJ (1977) Crustal anatexis: an experimental review. *Tectonophysics* 43: 41–71
- XIAOLIN X, ZHENHUA Z, JINCHU Z, BING R, MINGYUAN L (1998) Partitioning of F between aqueous fluids and albite granite melt and its petrogenetic and metallogenetic significance. *Chin J Geoch* 17: 303–310
- ZOPPIS-BRACCI L (1957) Geological study of the region Palacaguina and its antimony deposits. *Bol Servo Geol Nac, Nicaragua* 1: 29–34 (in Spanish)
- ZOPPIS-BRACCI L, DEL GIUDICE D (1961) Preliminary study of tungsten and molybdenum mineralization Macuelizo, Department of Nueva Segovia. *Bol Servo Geol Nac, Nicaragua* 5: 33–52 (in Spanish)
- ŽÁČEK V, HRADECKÝ P (2005) Geological map of Ocotal area (Nicaragua) 1 : 50 000. Czech Geological Survey, Prague (in Czech)